Myogenin controls via AKAP6 non-centrosomal microtubule organizing center formation at the nuclear envelope

Robert Becker[1], Silvia Vergarajauregui[1], Florian Billing[1], Maria Sharkova[1], Eleonora Lippolis[2], Kamel Mamchaoui[3], Fulvia Ferrazzi[2,4,5,6], Felix B. Engel[1,6,*]

[1]Experimental Renal and Cardiovascular Research, Department of Nephropathology, Institute of Pathology, Friedrich-Alexander-Universität Erlangen-Nürnberg (FAU), 91054 Erlangen, Germany

[2]Institute of Human Genetics, Friedrich-Alexander-Universität Erlangen-Nürnberg, 91054 Erlangen, Germany

[3]Sorbonne Universités UPMC Université Paris 06, INSERM U974, CNRS FRE3617, Center for Research in Myology, GH Pitié Salpêtrière, 47 Boulevard de l'Hôpital, 75013 Paris, France

[4]Department of Nephropathology, Institute of Pathology, Friedrich-Alexander-Universität Erlangen-Nürnberg (FAU), 91054 Erlangen, Germany

[5]Institute of Pathology, Friedrich-Alexander-Universität Erlangen-Nürnberg (FAU), 91054 Erlangen, Germany

[6]Muscle Research Center Erlangen (MURCE), 91054 Erlangen, Germany

Short title: Myogenin controls ncMTOC formation

***Corresponding author:**

Felix B. Engel, Universitätsklinikum Erlangen, Schwabachanlage 12 (TRC), 91054 Erlangen, Germany, felix.engel@uk-erlangen.de

Abstract

Non-centrosomal microtubule organizing centers (ncMTOC) are pivotal for the function of multiple cell types, but the processes initiating their formation are unknown. Here, we find that the transcription factor myogenin is required in myoblasts for recruiting centrosomal proteins. Moreover, myogenin is sufficient in fibroblasts for ncMTOC formation and centrosome attenuation. Bioinformatics combined with loss- and gain-of-function experiments identified induction of AKAP6 expression as one central mechanism for myogenin-mediated ncMTOC formation. Promoter studies indicate that myogenin preferentially induces the transcription of muscle- and ncMTOC-specific isoforms of *Akap6* and *Syne1*, which encodes nesprin-1α, the ncMTOC anchor protein in muscle cells. Overexpression of AKAP6β and nesprin-1α was sufficient to recruit endogenous centrosomal proteins to the nuclear envelope of myoblasts in the absence of myogenin. Taken together, our results illuminate how mammals transcriptionally control the switch from a centrosomal MTOC to an ncMTOC and identify AKAP6 as a novel ncMTOC component in muscle cells.

Keywords: myogenin; muscle differentiation; MTOC; non-centrosomal MTOC; AKAP6; centrosome; microtubules; terminal differentiation; nuclear envelope; transcription

45 **Introduction**

46 Correct organization of the microtubule cytoskeleton is essential for many cellular
47 processes such as the establishment of cell shape, organelle positioning or
48 intracellular transport (Akhmanova & Steinmetz, 2015; Conduit, Wainman, & Raff,
49 2015). In proliferating vertebrate cells, proteins that control microtubule nucleation and
50 anchoring accumulate as pericentriolar material at the centrosome, which in turn
51 functions as the dominant microtubule-organizing center (MTOC) (Prosser & Pelletier,
52 2015). The centrosomal MTOC is pivotal for cell cycle progression and correct
53 chromosome segregation during mitosis (Hinchcliffe, Miller, Cham, Khodjakov, &
54 Sluder, 2001; Khodjakov & Rieder, 2001; Sir et al., 2013). In contrast, MTOC function
55 is assigned to non-centrosomal sites during differentiation of various cell types
56 (Sanchez & Feldman, 2017). In epithelial cells, apically localized ncMTOCs participate
57 in organelle positioning and help to establish apical-basal cell polarity (Brodu, Baffet,
58 Le Droguen, Casanova, & Guichet, 2010; C. Lee, Scherr, & Wallingford, 2007; Meads
59 & Schroer, 1995; Toya et al., 2016). In neurons, dendritic branch points, Golgi outposts,
60 and pre-existing microtubules have been suggested to act as ncMTOC sites and
61 precise control of microtubule array polarity helps to define the axonal and dendritic
62 compartments (Luders, 2020; Nguyen et al., 2014; Ori-McKenney, Jan, & Jan, 2012;
63 Sanchez-Huertas et al., 2016). In striated (i. e. heart and skeletal) muscle cells,
64 ncMTOCs form at the nuclear envelope and contribute to correct nuclei positioning in
65 skeletal myotubes (Elhanany-Tamir et al., 2012; Espigat-Georger, Dyachuk, Chemin,
66 Emorine, & Merdes, 2016; Gimpel et al., 2017; Kronebusch & Singer, 1987; Tassin,
67 Maro, & Bornens, 1985).

68 Despite progress in illuminating identity, composition, and function of ncMTOCs, it
69 remains elusive which mechanisms initiate the switch from centrosomal to non-
70 centrosomal MTOCs during differentiation of vertebrate cells. The only mechanistic

71 insight into ncMTOC induction has been gained by studying *Drosophila* tracheal cells.
72 It was shown that the transcription factor trachealess, which specifies tracheal fate, is
73 required for the spastin-mediated release of centrosomal components from the
74 centrosome and their subsequent Piopio-mediated anchoring to the apical membrane
75 (Brodu et al., 2010).

76 Here, we aimed to identify a transcription factor that controls ncMTOC formation
77 in mammals utilizing skeletal muscle differentiation as an experimental system.
78 Mammalian skeletal muscle differentiation is controlled by a family of transcription
79 factors termed myogenic regulatory factors (MRFs) (Braun & Gautel, 2011;
80 Buckingham & Rigby, 2014). Among those, myoblast determination protein (MyoD)
81 regulates commitment to a myogenic fate and is thought to promote early differentiation
82 of myoblasts (Comai & Tajbakhsh, 2014; Ishibashi, Perry, Asakura, & Rudnicki, 2005).
83 The MRF myogenin acts as a unique regulator of terminal differentiation during
84 myogenesis. In the absence of myogenin *in vivo*, embryonic myofiber formation is
85 disturbed and the second wave of fetal myogenesis is largely abolished (Hasty et al.,
86 1993; Nabeshima et al., 1993; Venuti, Morris, Vivian, Olson, & Klein, 1995). Notably,
87 all MRFs are able to induce phenotypical markers of skeletal muscle in permissive non-
88 muscle cells (Braun, Bober, Winter, Rosenthal, & Arnold, 1990; Braun, Buschhausen-
89 Denker, Bober, Tannich, & Arnold, 1989; Comai & Tajbakhsh, 2014; Davis, Weintraub,
90 & Lassar, 1987; Edmondson & Olson, 1989; Weintraub et al., 1989). Therefore, we
91 examined whether MRFs regulate ncMTOC formation during skeletal muscle
92 differentiation and whether they are sufficient for ncMTOC initiation in non-muscle
93 cells.

94 Based on loss and gain of function experiments, quantitative analysis utilizing
95 different cell types, and promoter studies, we show here that myogenin is required and
96 sufficient for the formation of an ncMTOC at the nuclear envelope by controlling the

97 expression of muscle- and ncMTOC-specific isoforms of *Akap6* and *Syne1* which

98 encodes nesprin-1α.

99

100 **Results**

101 **Myogenin is required for centrosomal protein recruitment to the nuclear**
102 **envelope**

103 To elucidate the regulation of ncMTOC establishment in skeletal muscle cells, we
104 correlated the expression of MyoD and myogenin, transcription factors promoting early
105 (MyoD) or late (myogenin) muscle differentiation, with the ncMTOC formation during
106 mouse C2C12 myoblast differentiation. We analyzed two key steps during ncMTOC
107 formation: i) Expression of nesprin-1α, the nuclear envelope anchor for centrosomal
108 proteins (Espigat-Georger et al., 2016; Gimpel et al., 2017) and ii) recruitment of
109 PCM-1, the first centrosomal protein to localize to the nuclear membrane (Srsen, Fant,
110 Heald, Rabouille, & Merdes, 2009; Zebrowski et al., 2015). Immunofluorescence
111 analyses of C2C12 cells one day after induction of differentiation revealed that 49.1 ±
112 7% of nuclei were positive for MyoD, 12 ± 0.9% were positive for myogenin, 7.8 ± 0.3%
113 were positive for nesprin-1α, and 1.9 ± 0.3% were positive for PCM-1 (Figure 1A-C).
114 Note, PCM-1 recruitment to the nuclear envelope is a gradual process (Figure 1 –
115 figure supplement 1A). In our analysis intermediate stages were rare (<2% of total
116 PCM-1-positive nuclei) and have therefore been included in the total percentage of
117 PCM-1-positive nuclei.

118 All nuclei that were positive for PCM-1 were also positive for MyoD, myogenin, and
119 nesprin-1α (Figure 1B,E). This suggests that MyoD and/or myogenin might be required
120 for the recruitment of PCM-1 to the nuclear envelope. In contrast, only MyoD was
121 present in all nesprin-1α-positive nuclei whereas only 42% of nesprin-1α-positive
122 nuclei were also myogenin-positive (Figure 1A,D). Considering that nesprin-1α is
123 anchoring centrosomal proteins at the nuclear envelope, this suggests that myogenin
124 might be dispensable for ncMTOC formation.

125 To determine whether myogenin is dispensable for the establishment of the
126 ncMTOC, we depleted myogenin in C2C12 cells via siRNA and analyzed nesprin-1α
127 expression as well as nuclear envelope localization of the centrosomal proteins PCM-
128 1, pericentrin, and AKAP9, which is essential for microtubule nucleation at the nuclear
129 envelope, after two days of differentiation. The number of nesprin-1α-positive nuclei
130 was not significantly affected by myogenin depletion (Figure 1E,F). By contrast,
131 knockdown of myogenin reduced the number of PCM-1-positive nuclei from 11.6 ±
132 1.3% in control siRNA-treated cells to 2.3 ± 0.8% (Figure 1E,F). Similarly, pericentrin-
133 positive nuclei were reduced from 6.9 ± 0.1% to 1.4 ± 0.1% and AKAP9-positive nuclei
134 showed a reduction from 6.8 ± 0.5% to 1.4 ± 0.1% (Figure 1F and Figure 1 – figure
135 supplement 1B). Contrary to our hypothesis, these data indicate that myogenin is
136 required for centrosomal protein localization to the nuclear envelope during skeletal
137 muscle differentiation.

138 Considering that PCM-1 is 1) important for recruitment of other proteins to the
139 centrosome (Dammermann & Merdes, 2002; Prosser & Pelletier, 2020) and 2) the first
140 centrosomal protein to localize to the nuclear envelope {Srsen, 2009 #412}{Zebrowski,
141 2015 #419}, we aimed to assess whether the loss of PCM-1affects the recruitment of
142 other centrosomal proteins to the nuclear envelope. Depletion of PCM-1 reduced the
143 percentage of C2C12 nuclei fully or partially positive for pericentrin after two days of
144 differentiation from 5.8 ± 1% to 0.8 ± 0.2% and 2.7 ± 0.9% to 0.5 ± 0.1%, respectively
145 (Figure 1G,H). In contrast, PCM-1 depletion did not affect recruitment of AKAP9
146 (Figure 1 – figure supplement 1C). Similar qualitative results have been described in
147 myotubes (Espigat-Georger et al., 2016; Gimpel et al., 2017).

148 Collectively, our data suggest that the MyoD-driven early myogenic differentiation
149 is sufficient to induce nesprin-1α expression whereas myogenin regulates the nuclear
150 envelope targeting of AKAP9 and PCM-1, which in turn recruits pericentrin.

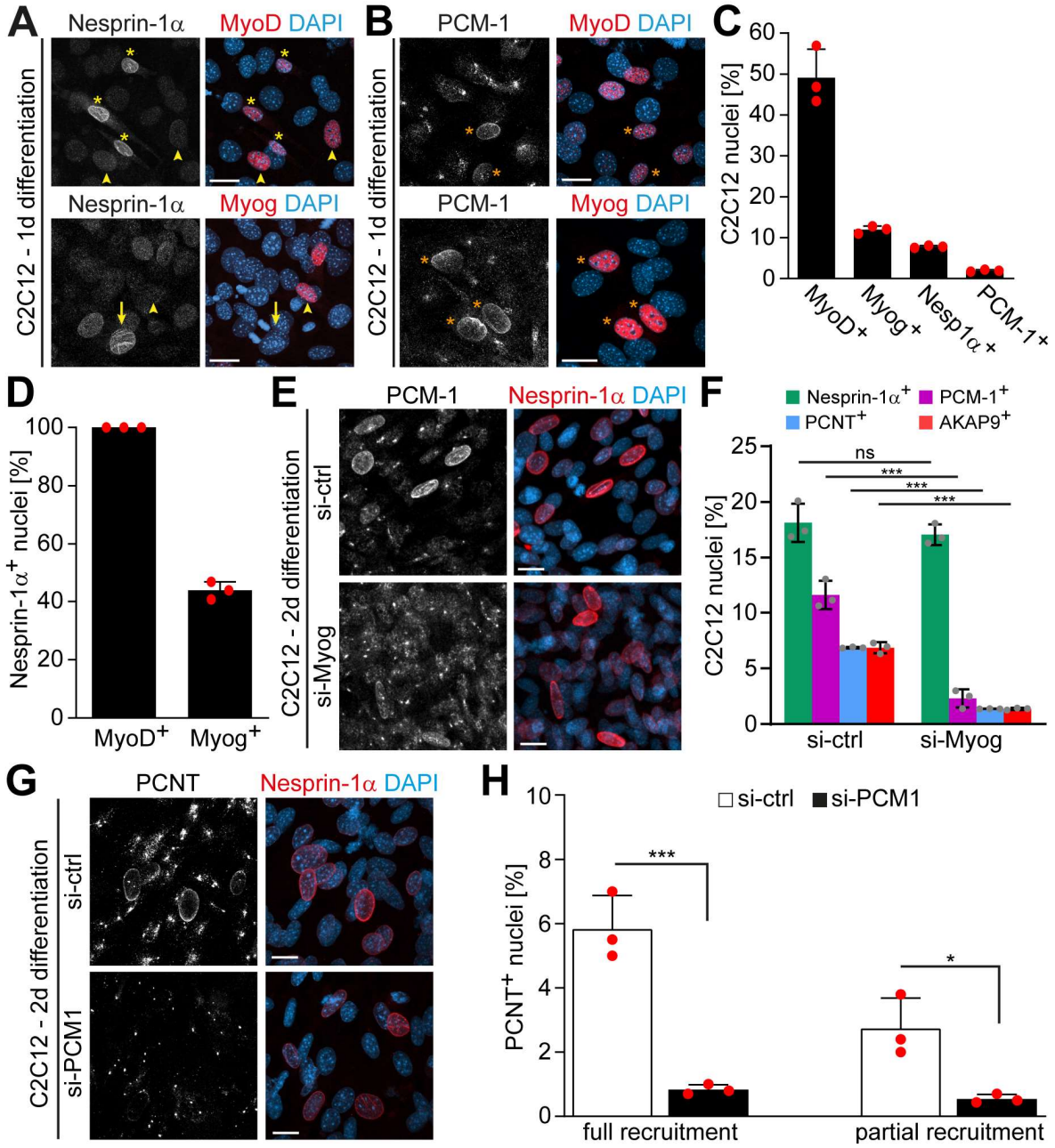

Figure 1. Myogenin is required for centrosomal protein recruitment to the nuclear envelope. **(A-B)** C2C12 cells were differentiated for one day and immunostained for the myogenic regulatory factors (MRFs) MyoD or myogenin (Myog) and nesprin-1α (A) or PCM-1 (B). Orange asterisks: MRF$^+$/PCM-1$^+$ nuclei; yellow asterisks: MRF$^+$/nesprin-1α$^+$ nuclei; arrowheads: MRF$^+$/nesprin-1α$^-$ nuclei; arrows: MRF$^-$/nesprin-1α$^+$ nuclei. Scale bars: 20 µm. **(C)** Quantification of (A) and (B). Data are represented as individual biological replicates, together with mean ± SD. **(D)** Quantification of MyoD and Myog in relation to nesprin-1α showing that not all nesprin-1α positive nuclei are myogenin positive. Data are represented as individual biological replicates, together with mean ± SD. **(E-F)** C2C12 myoblasts were transfected with negative control (si-ctrl) or myogenin siRNA (si-Myog) and differentiated for two days. Immunostaining (E) and subsequent quantification (F) shows that myogenin depletion affects nuclear recruitment of PCM-1, pericentrin (PCNT), and AKAP9 but not of nesprin-1α. 95% CI of differences si-Myog vs. si-ctrl = -3.11% to 0.98% (nesprin-1α$^+$), -11.31% to -7.22% (PCM-1$^+$), -7.53% to 3.43% (PCNT$^+$), -7.52% to -3.42% (AKAP9$^+$). Scale bars: 20 µm. **(G-H)** C2C12 myoblasts were transfected with si-ctrl or PCM-1 siRNA (si-PCM1) and differentiated for two days. PCNT was detected by immunostaining (G) and subsequent quantification (H) showed that PCM-1 depletion reduces PCNT$^+$ nuclei. 95% CI of differences si-PCM1 vs. si-ctrl = -6.6% to -3.4% (full), -3.78% to -0.59% (partial). Scale bars: 20 µm. Data are represented as individual biological replicates, together with mean ± SD. ns: $p > 0.05$. *: $p < 0.05$ ***: $p < 0.001$. n = 3.

170 **Ectopic myogenin expression is sufficient to induce a nuclear envelope MTOC**

171 All MRFs are able to "transdifferentiate" permissive non-muscle cells with varying
172 efficiency. They induce skeletal muscle markers such as the expression of contractile
173 proteins or cell fusion into myotubes (Braun et al., 1990; Braun et al., 1989; Davis et
174 al., 1987; Edmondson & Olson, 1989; Weintraub et al., 1989). However, ncMTOC
175 formation has never been analyzed in "transdifferentiated" cells. To determine whether
176 MRFs are sufficient to induce ncMTOC formation at the nuclear envelope in non-
177 muscle cells, we ectopically expressed MyoD-GFP, myogenin-GFP or GFP alone in
178 mouse NIH3T3 fibroblasts and analyzed the localization of PCM-1. NIH3T3 cells
179 transfected with GFP exhibited centrosomal PCM-1 localization, typical for proliferating
180 cells (Figure 2A). By contrast, expression of MyoD-GFP and myogenin-GFP induced
181 nuclear envelope localization of PCM-1 in a subset of GFP-positive cells (Figure 2A,B),
182 suggesting that both MRFs are sufficient individually to induce a switch from
183 centrosomal MTOC to a nuclear envelope MTOC.

184 The results obtained upon MyoD-GFP expression appear surprising, as our C2C12
185 experiments suggested that myogenin is required for centrosomal protein recruitment.
186 However, MyoD is known to activate myogenin transcription (Berkes & Tapscott,
187 2005). Analyzing endogenous myogenin expression in MyoD-GFP expressing cells,
188 we observed high myogenin levels in cells that had recruited PCM-1 to the nuclear
189 envelope compared to MyoD-GFP expressing cells where PCM-1 was absent from the
190 nuclear envelope (Figure 2 – figure supplement 1A). In addition, depletion of myogenin
191 in NIH3T3 cells abrogated the effect of MyoD-GFP expression on the recruitment of
192 PCM-1 to the nuclear envelope (Figure 2 – figure supplement 1B). This further argues
193 for myogenin to be required to recruit centrosomal proteins to the nuclear envelope.

194 In order to elucidate how myogenin induces nuclear envelope MTOC formation,
195 we generated stable NIH3T3 cell lines that express either mScarlet or myogenin-2A-

196 mScarlet (MYOG-mScarlet) under control of a tetracycline-responsive promoter (Tet-
197 ON). To induce myogenin expression and potentially centrosomal recruitment to the
198 nuclear envelope, we treated MYOG-mScarlet cells with doxycycline (Dox) for three
199 days. Immunofluorescence analysis revealed that Dox-treatment induced nuclear
200 envelope localization of PCM-1, pericentrin, and AKAP9 (Figure 2C, 2E, and 2G). To
201 better account for the dynamic of the recruitment process, we quantified the area of
202 the nuclear envelope positive for each centrosomal protein in mScarlet and MYOG-
203 mScarlet cells after Dox treatment (Figure 2D, 2F, and 2H). For this, we set an intensity
204 threshold for the centrosomal protein signal and quantified the percentage of pixels
205 above this threshold inside a 1 µm-wide band around the nucleus (identified by DAPI
206 signal). The signal at the centrosome, which localizes in close proximity to the nucleus
207 in most cells, accounts for the nuclear envelope coverage in mScarlet cells.
208 Quantification revealed that median PCM-1 nuclear envelope coverage increases from
209 12.5% in mScarlet cells to 30.3% in MYOG-mScarlet cells (Figure 2D). Pericentrin was
210 recruited with an increase of the median coverage from 8.2% in mScarlet cells to 23.1%
211 in MYOG-mScarlet cells (Figure 2F). AKAP9, which is essential for microtubule
212 nucleation at the nuclear envelope (Gimpel et al., 2017), coverage increased only
213 moderately from 3.6% to 6.2%, suggesting that AKAP9 recruitment is less efficient in
214 MYOG-mScarlet cells compared to PCM-1 and pericentrin (Figure 2H). However,
215 ~13% of analyzed MYOG-mScarlet nuclei showed a higher coverage than the
216 maximum observed in mScarlet-cells. Together, these data indicate that myogenin is
217 sufficient to induce nuclear envelope recruitment of centrosomal proteins in non-
218 muscle cells.

219 As nuclear envelope localization of centrosomal proteins requires nesprin-1α in
220 C2C12 cells (Espigat-Georger et al., 2016; Gimpel et al., 2017), we examined whether
221 myogenin is able to induce nesprin-1α expression in Dox-treated MYOG-mScarlet

222 cells. Dox-treatment resulted in nesprin-1-positive nuclei (Figure 2I) and RT-PCR
223 analysis confirmed that the α-isoform of nesprin-1 is upregulated upon myogenin
224 induction (Figure 2J). This indicate that while myogenin loss might be compensated by
225 another transcription factor in C2C12, myogenin can induce nesprin-1α expression.
226 Notably, chromatin immunoprecipitation (ChIP) sequencing data available through the
227 ENCODE consortium (Consortium et al., 2020; Yue et al., 2014) predict myogenin as
228 well as MyoD to bind a candidate regulatory element near the transcription start site of
229 nesprin-1α. To examine whether myogenin directly induces nesprin-1α transcription in
230 MYOG-mScarlet cells by binding to the α-isoform-specific promoter in the *Syne1* gene,
231 we performed ChIP, using an anti-myogenin antibody or an isotype control, followed
232 by PCR for the ENCODE-predicted site. PCR amplification was successful from
233 myogenin-precipitated DNA but not from IgG1 control (Figure 2K), indicating that
234 myogenin binds the nesprin-1α promoter and can induce expression of nesprin-1α in
235 permissive cells.

236 Finally, we examined if the myogenin-induced recruitment of centrosomal proteins
237 converts the nuclear envelope to a functional ncMTOC. For this we analyzed
238 microtubule regrowth after cold-induced depolymerization in Dox-treated mScarlet and
239 MYOG-mScarlet cells. In mScarlet-expressing cells, microtubule regrowth was
240 observed from the centrosome (Figure 2L). In contrast, MYOG-mScarlet cells exhibited
241 microtubule regrowth from the nuclear envelope to varying degrees. Quantification
242 revealed that median nuclear envelope coverage increased from 10.1% in mScarlet
243 cells to 18.4% in MYOG-mScarlet cells.

244 Collectively, these data demonstrate that myogenin is sufficient to induce ncMTOC
245 formation in NIH3T3 fibroblasts.

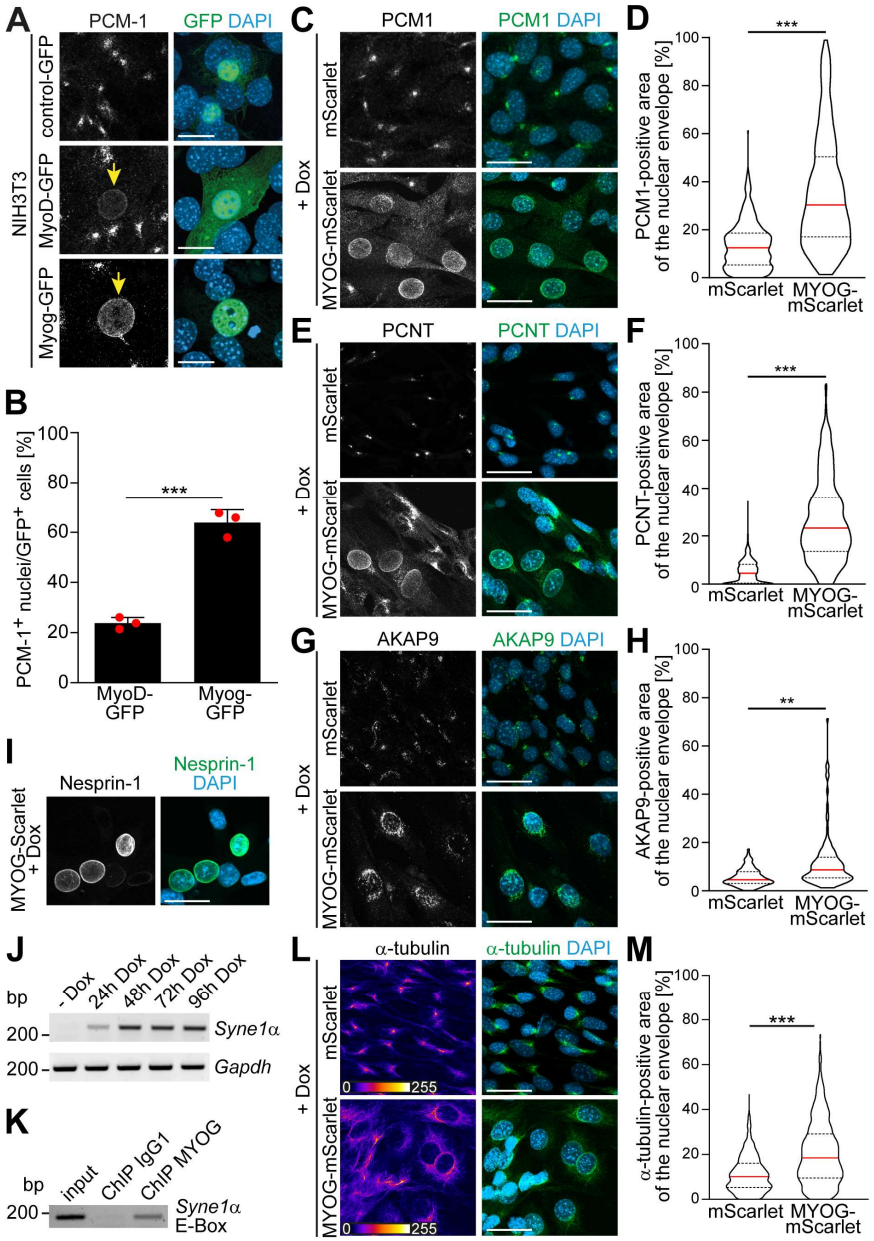

Figure 2. Myogenin expression is sufficient to induce ncMTOC formation in non-muscle cells. **(A)** NIH3T3 fibroblasts were transfected with constructs encoding GFP, MyoD-GFP or myogenin-GFP (Myog-GFP). After three days, PCM-1 localization was assessed by immunostaining. Arrows indicate nuclei of transfected cells which have recruited PCM-1. Scale bars: 10 µm. **(B)** Quantification of (A) demonstrating that myogenin induces nuclear recruitment of PCM-1 more efficiently than MyoD. Data are represented as individual biological replicates, together with mean ± SD. ***: $p < 0.001$; 95% CI of difference Myog-GFP vs. MyoD-GFP = 30.99% to 49.22%. n = 3. **(C-H)** NIH3T3 Tet-ON mScarlet or MYOG-2A-mScarlet (MYOG-mScarlet) cells were treated with doxycycline (Dox) for three days. After immunostaining, nuclear envelope recruitment of PCM-1 (C-D), pericentrin (Pcnt) (E-F), and AKAP9 (G-H) was analyzed and quantified. Data are depicted as violin plots. Red line indicates the median, dotted lines indicate the 25% and 75% percentile. ***: $p < 0.001$. Scale bars = 20 µm **(I)** Immunostaining of MYOG-mScarlet cells treated with Dox for three days showing the presence of nesprin-1α-positive nuclei. Scale bars = 20 µm **(J)** RT-PCR analysis of MYOG-mScarlet cells in the absence of Dox (-Dox) or treated with Dox for the indicated time points demonstrating that *Syne1α* is upregulated upon myogenin expression. *Gapdh* was used as equal input control. **(K)** ChIP-PCR analysis of Dox-treated MYOG-mScarlet cells using an anti-myogenin antibody or an IgG1 control showing that myogenin binds an E-box in the *Syne1α* promoter region. **(L-M)** Immunostaining of α-tubulin and subsequent quantification of nuclear envelope coverage after 30s of microtubule regrowth following cold-induced microtubule depolymerization in mScarlet or MYOG-mScarlet cells treated with Dox for three days. Data are depicted as violin plots. Red line indicates the median, dotted lines indicate the 25% and 75% percentile. ***: $p < 0.001$. Scale bars = 20 µm.

268 **Myogenin expression attenuates the centrosomal MTOC**

269 In different cell types, it has been observed that ncMTOC formation is associated with
270 attenuation of the centrosomal MTOC (Leask, Obrietan, & Stearns, 1997; Nguyen,
271 Stone, & Rolls, 2011; Yang & Feldman, 2015; Zebrowski et al., 2015). Therefore, we
272 examined if myogenin expression induces centrosome attenuation in MYOG-mScarlet
273 fibroblasts. Dox stimulation resulted in a significant reduction of pericentrin levels at
274 centrioles in MYOG-mScarlet cells when compared to Dox-treated mScarlet cells
275 (Figure 3A,B). In contrast, levels of Cep135, a centriole-associated protein, which does
276 not relocalize to the nuclear envelope in muscle cells, did not change significantly upon
277 myogenin induction (Figure 3C,D) indicating that myogenin affects centrosomal
278 localization of PCM proteins but not of centriole-associated proteins. To test if
279 myogenin attenuates MTOC activity at the centrosome, we analyzed centrosomal
280 levels of the microtubule nucleating factor γ-tubulin. Induced MYOG-mScarlet cells
281 displayed a significant reduction in centrosomal γ-tubulin levels compared to mScarlet
282 control cells (Figure 3E). Analyzing microtubule regrowth, we observed that
283 centrosomes still nucleated microtubules in MYOG-mScarlet cells that exhibited
284 microtubule nucleation at the nuclear envelope (Figure 3F). However, α-tubulin signal
285 at centrioles was less intense in MYOG-mScarlet cells compared to mScarlet cells,
286 indicating a reduced MTOC activity (Figure 3F). Taken together, these data indicate
287 that myogenin expression – in parallel to inducing ncMTOC formation – attenuates the
288 centrosomal MTOC and that centrosomal and nuclear envelope MTOC can be active
289 at the same time.

290

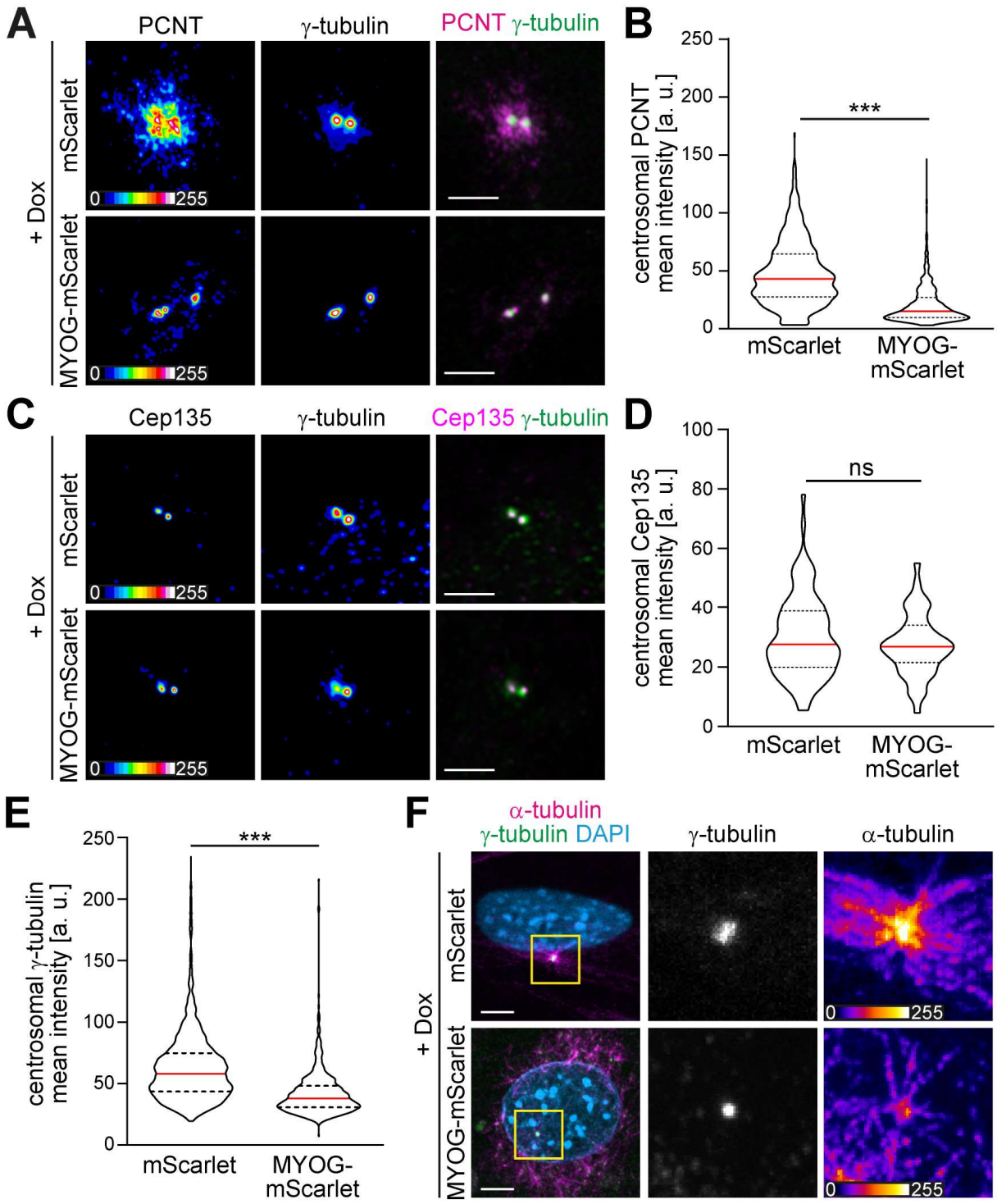

Figure 3. Myogenin expression attenuates the centrosomal MTOC
(A-E) mScarlet or MYOG-mScarlet cells were stimulated with Dox for three days and pericentrin (Pcnt) (A), Cep135 (C), and γ-tubulin (A, C) were detected by immunostaining. Quantification shows that pericentrin (B) and γ-tubulin (E) intensities at the centrosome are reduced upon myogenin induction while Cep135 intensity (D) is not significantly affected. Single channel images of Pcnt, γ-tubulin, and Cep135 are false-colored to visualize different intensities. Data are shown as violin plots. The red line indicates the median and dotted lines indicate the 25% and 75% percentile. ns: $p > 0.05$. ***: $p < 0.001$. Scale bars = 5 µm **(F)** Immunostaining of α-tubulin and γ-tubulin in Dox-stimulated mScarlet or MYOG-mScarlet cells after 30s of microtubule regrowth. Intensity-based color-coding of α-tubulin shows that microtubule growth from centrioles is reduced after myogenin induction. Scale bars = 5 µm.

303 **AKAP6 is a potential mediator of myogenin-induced ncMTOC formation**

304 The myogenin depletion experiments suggested that the sole presence of nesprin-1α
305 at the nuclear envelope does not allow efficient recruitment of MTOC components
306 during muscle differentiation (Figure 1F). Thus, myogenin potentially contributes to the
307 recruitment process by controlling the expression of proteins that are necessary for
308 1) inhibiting the localization of centrosomal proteins to the centrosome, 2) targeting
309 centrosomal proteins to the nucleus, and/or 3) anchoring centrosomal proteins to the
310 nuclear envelope via nesprin-1α.

311 In order to identify candidates that act downstream of myogenin and mediate
312 ncMTOC formation, we integrated published myogenin ChIP-Seq data (Yue et al.,
313 2014) with RNA-Seq data of C2C12 differentiation (Doynova, Markworth, Cameron-
314 Smith, Vickers, & O'Sullivan, 2017) (Figure 4A). Myogenin ChIP-Seq data was
315 obtained at four different time points (myoblasts, 24 h differentiation, 60 h
316 differentiation, and 7 days differentiation; see Methods section for details) whereas the
317 RNA-Seq data-set contained three time points (myoblasts as well as differentiating
318 C2C12 cells at 3 days and 7 days of differentiation). PCM-1 nuclear envelope
319 localization can already be observed 24 h after induction of differentiation (Figure 1A),
320 but the number of cells which differentiate and form an ncMTOC increases over time.
321 Additionally, we assumed genes required for the maintenance of the ncMTOC in
322 differentiated cells have to be actively transcribed. Therefore, we considered only
323 those myogenin binding sites in our analysis which were detected in the ChIP-Seq
324 data-set at 24 h, 60 h, and 7 days of differentiation. The promoters of 2462 genes were
325 bound by myogenin at these three time points (Figure 4B). We then intersected these
326 2462 genes with a list of 3800 genes, which were upregulated in the RNA-Seq data-
327 set at both 3 days and 7 days of differentiation when compared to proliferating
328 myoblasts (Figure 4B). This intersection yielded a list of 748 potential direct myogenin

329 target genes (Figure 4B). Considering that skeletal muscle cells and cardiomyocytes
330 (myogenin-negative) both express nesprin-1α and exhibit a nuclear envelope MTOC,
331 we hypothesized that ncMTOC formation in both cell types is controlled by similar
332 mechanisms. Thus, we assessed whether any of the 748 target genes are upregulated
333 during rat heart development from embryonic day 15 to postnatal day 3, the
334 developmental window in which ncMTOCs form in cardiomyocytes (Zebrowski et al.,
335 2015). For this purpose, we utilized a microarray-derived temporal expression data-set
336 spanning rat heart development (Patra et al., 2011). This strategy helped to further
337 reduce the number of candidate genes to 107 myogenin targets that potentially
338 mediate ncMTOC formation (Supplementary file 1). As our previous data suggested
339 that nesprin-1α alone does not allow efficient recruitment of centrosomal proteins to
340 the nuclear envelope, we first focused on candidates that potentially cooperate with
341 nesprin-1α in anchoring centrosomal proteins to the nuclear envelope. To this end, we
342 utilized Gene Ontology analysis to identify candidates that are annotated to localize at
343 the nuclear envelope (Figure 4A). Four genes matched the Gene Ontology cellular
344 component search terms “nuclear membrane” and “nuclear envelope”: *Akap6*, *Dmpk*,
345 *Rb1cc1*, and *Tmem38a*. Previous studies indicated that myogenin directly binds and
346 activates the promoter of *Akap6* (S. W. Lee et al., 2015), which encodes the large
347 scaffold A-kinase anchoring protein (AKAP) 6 (also known as mAKAP). AKAP6 has
348 been described to localize to the nuclear envelope of cardiomyocytes through
349 interaction with the N-terminal spectrin domains of nesprin-1α and to act as a signaling
350 hub by assembling signaling proteins such as protein kinase A, ryanodine receptor,
351 phosphodiesterase 4D3 and phospholipase C (Kapiloff, Schillace, Westphal, & Scott,
352 1999; Pare, Easlick, Mislow, McNally, & Kapiloff, 2005; Passariello, Li, Dodge-Kafka,
353 & Kapiloff, 2015; Ruehr et al., 2003). Furthermore, proximity labeling indicated that
354 AKAP6 is an interactor of nesprin-1α in C2C12 myotubes (Gimpel et al., 2017). Taken

355 together, these data identify AKAP6 as a potential mediator of myogenin-induced
356 ncMTOC formation.

357 AKAP6 occurs in two isoforms: The brain-specific α-isoform and the β-isoform,
358 which is predominantly expressed in heart and skeletal muscle (Michel et al., 2005).
359 We first determined if myogenin binds the β-isoform promoter of *Akap6* in MYOG-
360 mScarlet fibroblasts and if AKAP6β expression is induced in these cells upon Dox
361 treatment. We could amplify an E-Box containing region of the β-isoform promoter after
362 ChIP using an anti-myogenin antibody (Figure 4C). RT-PCR analysis showed that
363 AKAP6β is upregulated after Dox stimulation (Figure 4D). This indicates that, in
364 fibroblasts, myogenin can bind the *Akap6*β-isoform promoter and induce AKAP6
365 expression.

366 To determine whether nesprin-1α is – similar to the situation in cardiomyocytes –
367 involved in AKAP6β localization to the nuclear envelope of skeletal muscle cells (Pare
368 et al., 2005), we analyzed the expression pattern of AKAP6 (refers to the β isoform if
369 not specified) and nesprin-1α in C2C12 cells. Immunofluorescence analysis at two
370 days differentiation showed that all AKAP6-positive nuclei were nesprin-1α-positive
371 (Figure 4E). In addition, high-resolution microscopy suggested that AKAP6 mainly
372 localizes at the cytoplasmic side of nesprin-1α (Figure 4F and Figure 4 – figure
373 supplement 1). It has been reported that the C-terminus of nesprin-1α is inserted into
374 the outer nuclear membrane, whereas the N-terminus extends into the cytoplasm
375 (Apel, Lewis, Grady, & Sanes, 2000; Q. Zhang et al., 2001).

376 To test if nesprin-1α is required to anchor AKAP6 to the nuclear envelope, patient-
377 derived myoblasts carrying a mutation in the *SYNE1* gene (23560 G>T causing a
378 premature stop and loss nesprin-1α expression) and myoblasts of healthy donors were
379 differentiated into myotubes and AKAP6 localization was compared (Figure 4G).
380 Whereas nesprin-1α and AKAP6 localized to the nuclear envelope of myotubes from

healthy donors, expression of nesprin-1α and nuclear membrane localization of AKAP6 were abolished in myotubes carrying the *SYNE1* mutation. Taken together, these data indicate that AKAP6 localizes to the nuclear envelope in differentiated skeletal muscle cells via interaction with nesprin-1α.

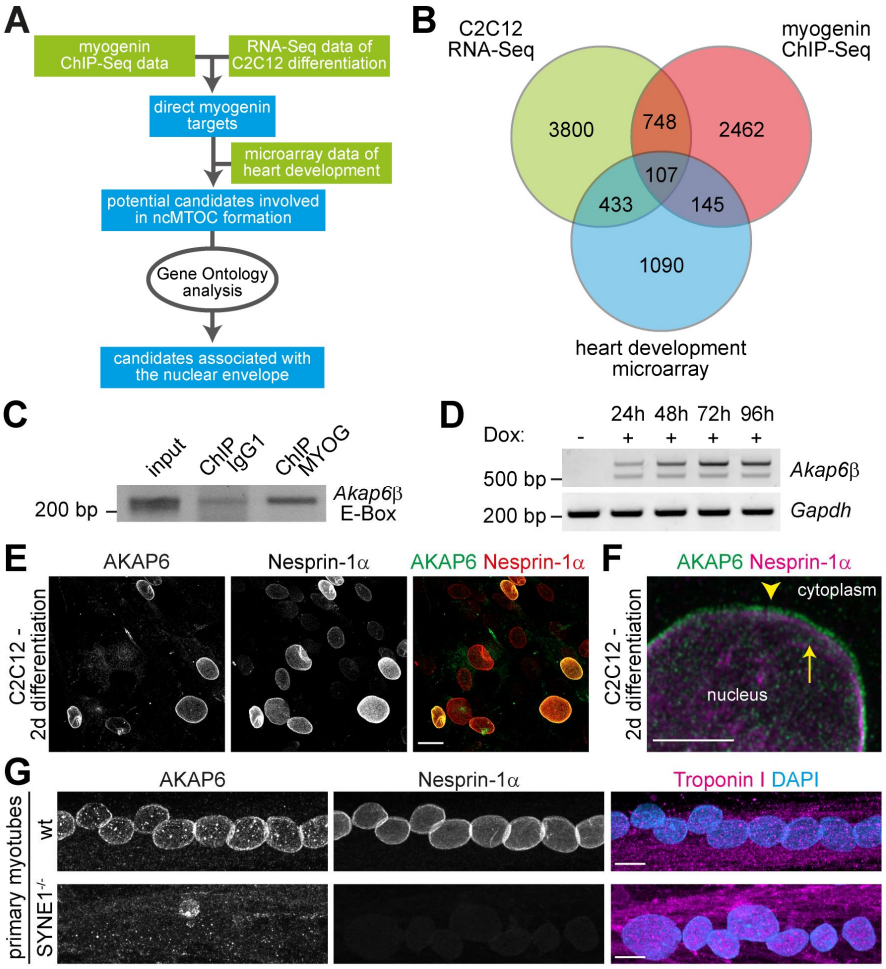

Figure 4. The nesprin-1α interaction partner AKAP6 is a potential mediator of myogenin-induced ncMTOC formation.

(A) Scheme illustrating the bioinformatics workflow used to identify potential myogenin downstream candidates. **(B)** Venn diagram depicting the numbers of genes matching criteria for the individual data sets and for intersection of data sets. Criteria for Myogenin ChIP-Seq data (red): Genes where myogenin binding was detected at the promoter region; criteria for C2C12 RNA-Seq data (green) and for microarray data of rat heart development (blue): up-regulated genes. **(C)** ChIP-PCR analysis of Dox-treated MYOG-mScarlet cells using an anti-myogenin antibody or an IgG1 control showing that myogenin binds an E-box in the *Akap6* β-promoter region. **(D)** RT-PCR analysis of MYOG-mScarlet cells in the absence of Dox (-Dox) or treated with Dox for the indicated time points demonstrating that *Akap6β* is upregulated upon myogenin expression. The two bands for *Akap6β* derive from alternative splicing of the first exon of *Akap6β* which results in a ~200 bp insertion in the 5' untranslated region. *Gapdh* was used as equal input control. **(E)** C2C12 cells were differentiated for two days and immunostaining shows that all AKAP6^{+} nuclei are also nesprin-1α^{+}. Scale bar: 20 µm. **(F)** High resolution Airyscan image of (E). Arrowhead indicates AKAP6 localized at the cytoplasmic side of nesprin-1α signal. Arrow marks nesprin-1α that is localized at the nuclear side of AKAP6 signal. Scale bar: 0.5 µm. **(G)** Myoblasts from healthy donors (wt) and from patients carrying a mutation in the *SYNE1* gene (SYNE1$^{-/-}$) were differentiated for four days. Immunostaining analysis showed that loss of nesprin-1α is associated with loss of AKAP6 from the nuclear envelope in differentiated myotubes (troponin I). Scale bars: 10 µm.

406 **AKAP6 is required for ncMTOC formation and maintenance**

407 To examine the role of AKAP6 in ncMTOC formation we performed siRNA-mediated
408 depletion experiments in differentiating C2C12 cells and MYOG-mScarlet fibroblasts.
409 In C2C12 cultures differentiated for two days, 12.3 ± 0.6% of nuclei were positive for
410 AKAP6 and 10.4 ± 1.2% of nuclei were positive for PCM-1 (Figure 5A,B). Importantly,
411 AKAP6 was found at all nuclei that had recruited PCM-1. Transfection of differentiating
412 C2C12 cultures with AKAP6 siRNA significantly reduced the number of AKAP6-
413 positive nuclei from 12.3 ± 0.6% to 4.8 ± 0.1% and the number of PCM-1-positive
414 nuclei from 10.4 ± 1.2% to 3.4 ± 0.3% (Figure 5B) but had no effect on nesprin-1α
415 localization (Figure 5 - figure supplement 1). Correspondingly, treatment of Dox-
416 induced MYOG-mScarlet with AKAP6 siRNA decreased median nuclear envelope
417 coverage by PCM-1 and pericentrin from 22.6% to 9% and 18.7% to 5.5%, respectively
418 (Figure 5C-E). Median coverage of AKAP9 was only moderately affected (7.2% to
419 6.5%) but nuclei showing more than ~18% AKAP9 coverage were completely lost after
420 AKAP6 depletion (Figure 5F). Next, we examined if AKAP6 promotes nuclear envelope
421 recruitment by directly interacting with centrosomal proteins. For this, we performed
422 co-immunoprecipitation experiments using an anti-AKAP6 antibody. We could co-
423 precipitate PCM-1 from MYOG-mScarlet lysates but not from mScarlet lysate (Figure
424 5G). These data indicate that AKAP6 is required for the localization of centrosomal
425 proteins to the nuclear envelope, in part by interacting with PCM-1.

426 To determine if AKAP6 is required for maintaining MTOC protein localization at the
427 nuclear envelope, we transfected C2C12 cultures enriched for myotubes with AKAP6
428 siRNA (Figure 5G,H). Depletion of AKAP6 resulted in the loss of PCM-1, AKAP9, and
429 pericentrin from the nuclear envelope in myotubes.

430 Taken together, our data demonstrate that AKAP6 is required for recruiting
431 centrosomal proteins to the nuclear envelope as well as maintaining nuclear envelope

localization of centrosomal proteins in myotubes, most likely by acting as an adaptor between centrosomal proteins and the nuclear membrane anchor nesprin-1α.

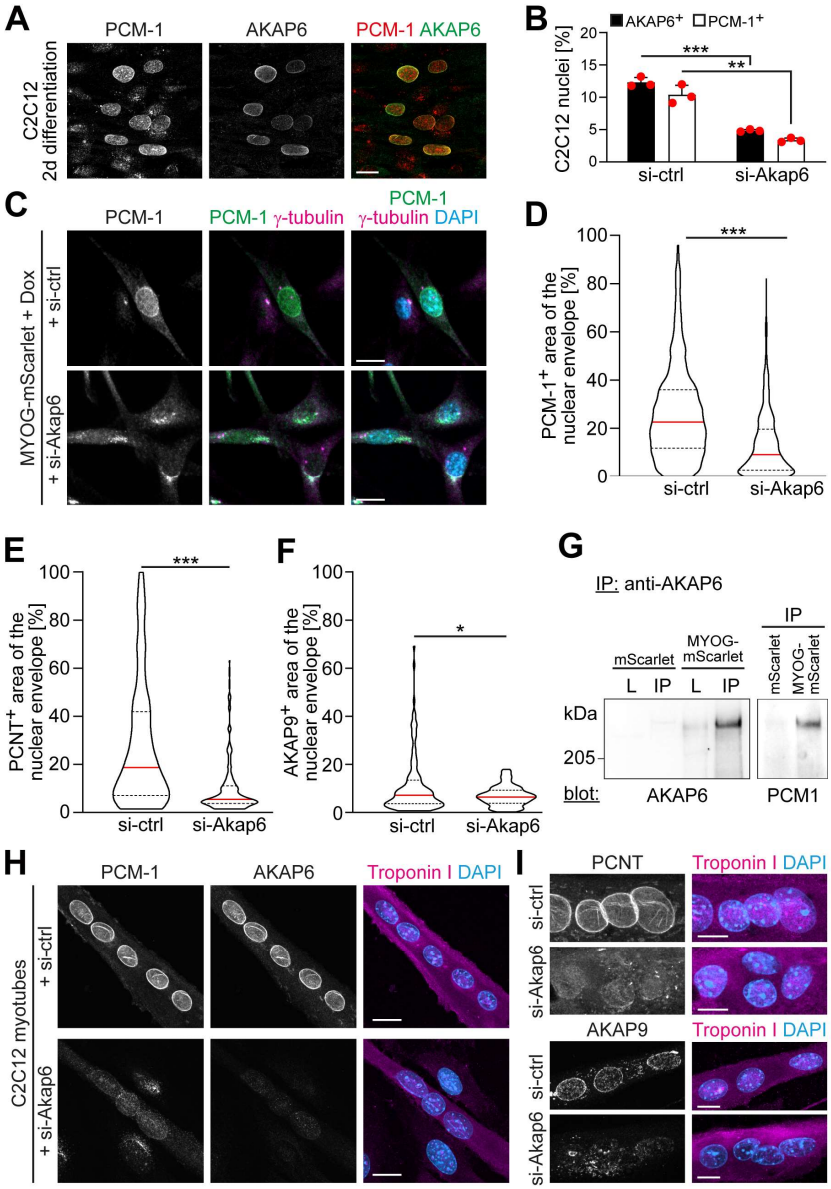

Figure 5. AKAP6 is required for nuclear envelope localization of centrosomal proteins. **(A)** C2C12 cells were differentiated for two days. Immunostaining shows that all PCM-1⁺ nuclei are also AKAP6⁺. Scale bar: 20 µm. **(B)** Quantification of AKAP6⁺ and PCM-1⁺ nuclei in C2C12 cells treated with negative control (si-ctrl) or Akap6 (si-Akap6) siRNA after two days of differentiation indicate that AKAP6 is required for nuclear PCM-1 localization. Data are represented as individual biological replicates, together with mean ± SD. **: $p = 0.0012$, 95% CI = 6.21% to 8.74%; ***: $p < 0.0001$, 95% CI = 4.63% to 9.43%. n = 3. **(C)** MYOG-mScarlet cells were treated with si-ctrl or si-Akap6 and subsequently treated with Dox for three days. Image analysis revealed that myogenin-induced recruitment of PCM-1 to the nuclear envelope is AKAP6-dependent. Scale bars: 10 µm. **(D)** Quantification of (C). Data are shown as violin plots. The red line indicates the median and dotted lines indicate the 25% and 75% percentile. ***: $p < 0.001$. **(E-F)** Quantification of pericentrin (E) and AKAP9 (F) nuclear coverage in Dox-stimulated MYOG-mScarlet cells treated with si-ctrl or si-Akap6. Data are shown as violin plots. The red line indicates the median and dotted lines indicate the 25% and 75% percentile. *: $p < 0.05$. ***: $p < 0.001$. **(G)** Co-Immunoprecipitation (IP) of PCM-1 from MYOG-mScarlet but not from mScarlet lysate (L) using an anti-AKAP6 antibody. **(H-I)** Enriched C2C12 myotubes (troponin I) were transfected with negative control (si-ctrl) or Akap6 (siAkap6) siRNA and immunostaining demonstrates that AKAP6 is required for maintaining nuclear envelope localization of PCM-1 (H) as well as pericentrin and AKAP9 (I). Scale bars (H): 20 µm, (I): 10 µm.

453 **AKAP6 is required for ncMTOC function**

454 The nuclear envelope MTOC has been described to be required for correct positioning
455 and distribution of nuclei in multinucleated myotubes via two different mechanisms: 1)
456 PCM-1 enables the recruitment of the dynein regulator p150glued and other motor
457 proteins to the nuclear envelope and promotes alignment of nuclei (Espigat-Georger
458 et al., 2016), and 2) the Akap9-dependent nucleation of microtubules from the nuclear
459 envelope contributes to the spreading of nuclei throughout the cell body (Gimpel et al.,
460 2017) (Figure 6A). Our results indicate a potential role for AKAP6 in both aspects of
461 nucleus positioning as it is required for PCM-1 and AKAP9 to localize to the nuclear
462 envelope. Analyzing the positioning and distribution of nuclei in enriched C2C12
463 myotubes two days after siRNA-mediated depletion of AKAP6, we found that AKAP6
464 depletion reduced the number of myotubes with aligned nuclei (66.0 ± 7.5% to 34.7 ±
465 7.6%) and increased the number of myotubes with overlapping nuclei (26.0 ± 6.5% to
466 58.3 ± 9.6%), compared to control myotubes (Figure 6B,C). This indicates that AKAP6
467 is required for proper alignment and spreading of nuclei in myotubes.

468 Next, we aimed to confirm that the observed nuclei mispositioning in AKAP6-
469 depleted cells is due to aberrant microtubule nucleation and motor protein recruitment
470 at the nuclear envelope. Immunofluorescence analysis showed that two days post
471 siRNA transfection the microtubule network organization was similar in AKAP6-
472 depleted and control myotubes showing the typical organization of microtubules in
473 longitudinal arrays (Figure 6 – figure supplement 1A). Similar results have been
474 obtained previously when depleting nesprin-1α (Espigat-Georger et al., 2016). Yet, we
475 observed that AKAP6 depletion resulted in a reduced intensity of detyrosinated (i.e.
476 stable) microtubules compared to control myotubes (Figure 6 – figure supplement 1B).
477 To test if AKAP6 depletion affects the nucleation of new microtubules, we assessed
478 microtubule regrowth after nocodazole-induced depolymerization in C2C12 myotubes.

479 In myotubes treated with control siRNA, microtubules regrew from the nuclear
480 envelope and to a lesser extent from cytoplasmic loci (Figure 6D). In AKAP6-depleted
481 myotubes, microtubule regrowth from the nuclear envelope was abolished (Figure 6D).
482 This suggests that AKA6 depletion impairs spreading of myonuclei by preventing
483 microtubule growth from the nuclear envelope. Next, we analyzed the localization of
484 p150glued (also known as DCTN1). In control siRNA-treated myotubes, p150glued
485 localized at the nuclear envelope (Figure 6E). AKAP6 depletion resulted in a reduction
486 of p150glued at the nuclear envelope of C2C12 myotubes (Figure 6E) suggesting that
487 the reduced number of myotubes with aligned nuclei is due to impaired dynein
488 activation. Collectively, these data demonstrate that AKAP6 is required for the function
489 of the nuclear envelope MTOC in skeletal muscle cells.
490

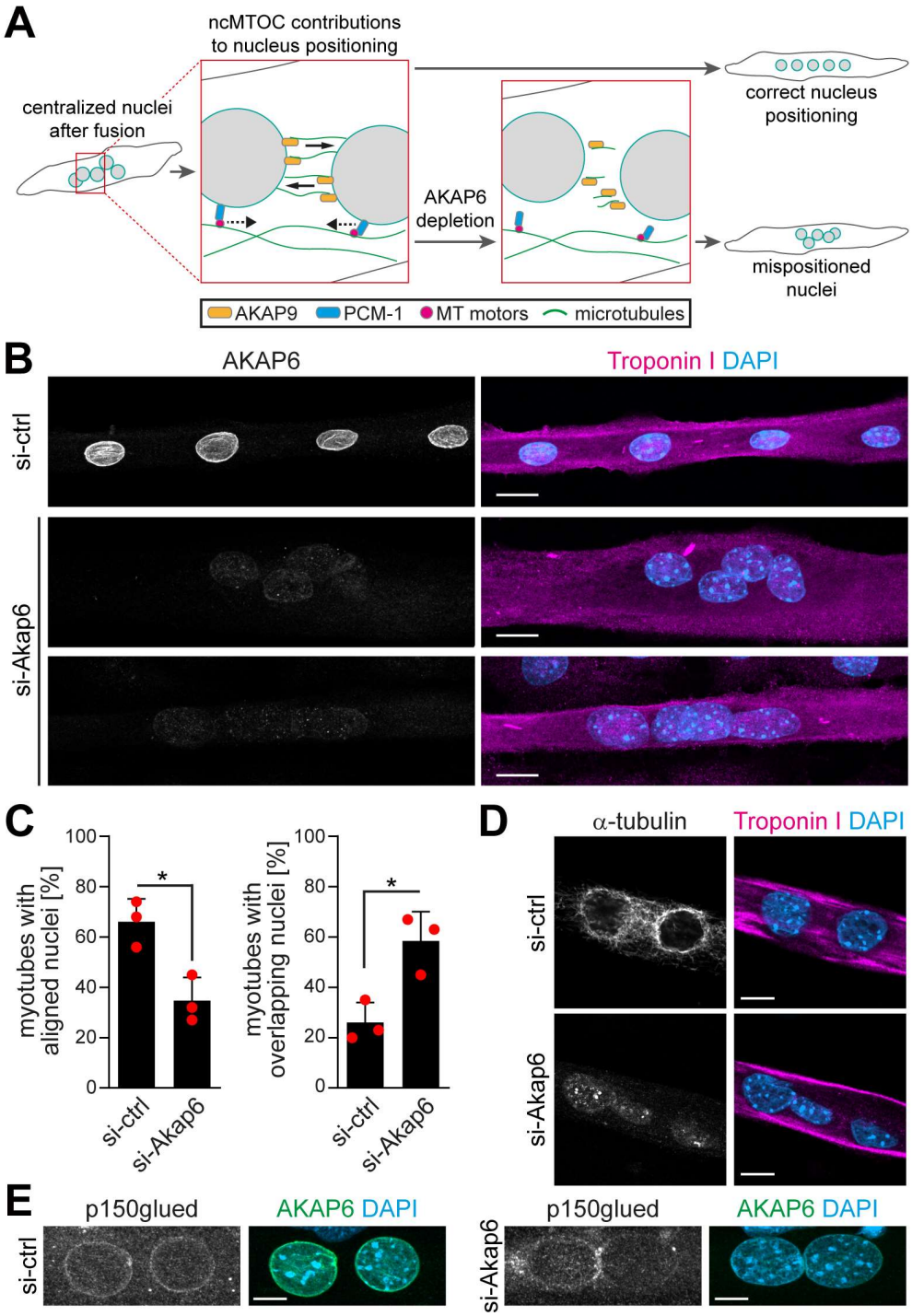

Figure 6. AKAP6 is required for correct nuclear positioning in myotubes.
(A) Scheme illustrating the role of the ncMTOC in myonuclear positioning and the potential impact of AKAP6 depletion. **(B)** Enriched C2C12 myotubes (troponin I) were transfected with negative control (si-ctrl) or Akap6 (si-Akap6) siRNA. The upper si-Akap6 panel shows a representative image of a myotube with misaligned nuclei, the lower si-Akap6 panel shows nuclei overlapping inside a myotube. Scale bars: 20 µm. **(C)** Quantification of (B). Data are represented as individual biological replicates, together with mean ± SD. *: $p < 0.05$, 95% CI of difference si-Akap6 vs. si-ctrl = 10.42% to 52.25% (left graph); 95% CI = 9.65% to 55.02% (right graph). n = 3. **(D)** Enriched C2C12 myotubes (troponin I) were transfected with si-ctrl or si-Akap6 and subsequently subjected to a nocodazole-based microtubule (α-tubulin) regrowth assay. Image analysis showed that AKAP6 depletion abrogated microtubule nucleation at the nuclear envelope. Scale bars: 10 µm. **(E)** Enriched C2C12 myotubes (troponin I) transfected with si-ctrl or si-Akap6 were immunostained for the dynein regulator p150glued. Image analysis showed that AKAP6 depletion reduces p150glued signal at the nuclear envelope. Scale bars: 5 µm.

507 **Myogenin-induced isoforms of nesprin-1 and AKAP6 are sufficient for**
508 **centrosomal protein recruitment**

509 To examine if myogenin specifically induces expression of isoforms that are associated
510 with the nuclear envelope MTOC in skeletal muscle, we performed ChIP on MYOG-
511 mScarlet cell lysate using an anti-myogenin antibody and assessed the abundance of
512 isoform-specific promoter regions of *Syne1* and *Akap6* in the precipitated DNA. For
513 this, we performed semi-quantitative PCR (qPCR) using primer pairs targeting
514 myogenin consensus binding sites (i.e. E-boxes) in regions predicted by ENCODE
515 data (Consortium et al., 2020) to be associated with myogenin binding (Figure 7A,C).
516 We found that the amount of template corresponding to the promoter region upstream
517 of the nesprin-1α transcript (nesprin-1α2) was 4.5-fold higher than the promoter region
518 of the long nesprin-1 isoform (nesprin-1-giant) (Figure 7B). Similarly, the promoter
519 region upstream of the AKAP6β transcript was 3-fold enriched compared to the
520 promoter region of the AKAP6α transcript (Figure 7D). This indicates that myogenin
521 preferentially binds promoter regions of *Syne1* and *Akap6* isoforms that are involved
522 in ncMTOC formation.

523 To test if the preferential binding is associated with an increased activation of
524 transcription of specific isoforms, we constructed vectors with putative promoter
525 regions of AKAP6α, AKAP6β, nesprin-1-giant, or nesprin-1α located directly upstream
526 of a luciferase coding sequence and transfected them into human HEK293T cells
527 together with GFP or myogenin-GFP. Co-transfection of myogenin with the AKAP6β
528 promoter construct increased luciferase activity 10.9-fold, while co-transfection with
529 the AKAP6α promoter construct did not show a significant increase compared to GFP-
530 transfected control (Figure 7E). Similarly, we observed a 21.7-fold increase in activity
531 when myogenin was co-transfected with the nesprin-1α promoter construct but only a
532 mild 2.7-fold increase after co-transfection with the promoter construct of nesprin-1-

533 giant (Figure 7F). These results indicate that myogenin preferentially induces
534 transcription of nesprin-1α and AKAP6β.

535 Finally, we examined whether the myogenin-induced isoforms of nesprin-1 and
536 AKAP6 are sufficient to recruit centrosomal proteins in the absence of myogenin. For
537 this, we expressed nesprin-1α-mCherry alone or together with AKAP6β-GFP in
538 undifferentiated, myogenin-negative myoblasts. In nesprin-1α-mCherry-transfected
539 cells, PCM-1 did not localize to the nuclear envelope (Figure 7G). In contrast, co-
540 transfection of nesprin-1α-mCherry and AKAP6β-GFP was sufficient to recruit PCM-1
541 to the nuclear envelope (Figure 7G).

542 Taken together, our results demonstrate that myogenin specifically induces
543 transcription of isoforms which are 1) required for the ncMTOC in differentiated skeletal
544 muscle cells and 2) sufficient to recruit centrosomal proteins to the nuclear envelope
545 in cells with a centrosomal MTOC.

546
547

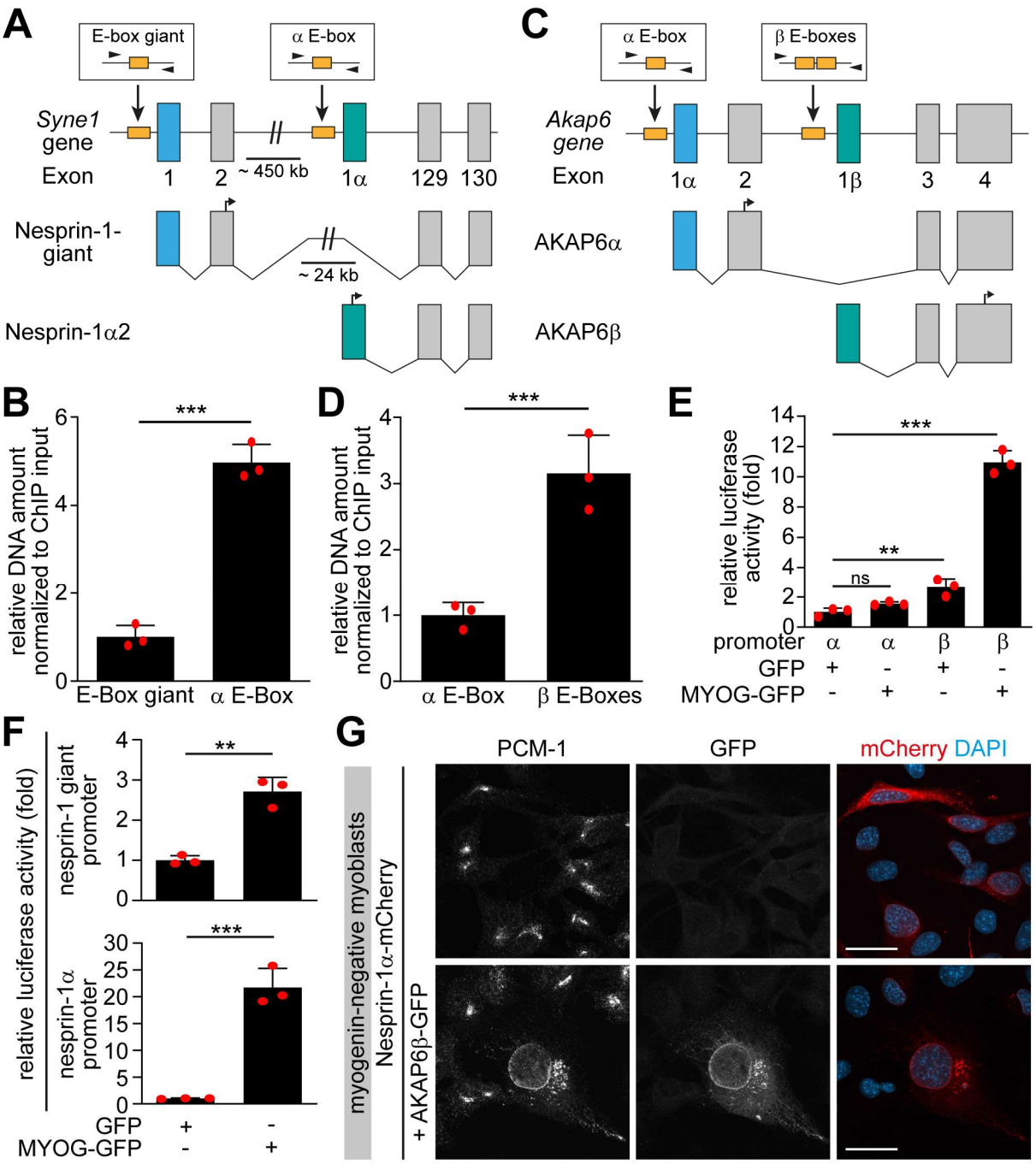

Figure 7. Myogenin preferentially induces MTOC-associated isoforms of *Syne1* and *Akap6*. **(A, C)** Schematic representation of the murine *Syne1* (A) and *Akap6* (C) gene and derived transcripts. Exons are indicated by grey rectangles and the first exon of each transcript is marked by color. E-boxes (myogenin consensus sites) inside putative promoters are indicated as yellow boxes and small black arrows mark the primers used for qPCR. **(B, D)** Myogenin ChIP from Dox-stimulated MYOG-mScarlet cells followed by qPCR for the indicated E-boxes shows that myogenin preferentially binds the promoter regions upstream of *nesprin-1α2* and *Akap6β* transcripts. Data are represented as individual biological replicates, together with mean ± SD. ***: $p < 0.001$. **(E-F)** Luciferase assay testing the activity of the indicated *Akap6* (E) or *Syne1* (F) promoters in the presence of GFP or myogenin-GFP (MYOG-GFP). Data are represented as individual biological replicates, together with mean ± SD. ns: $p > 0.05$. **: $p < 0.01$. ***: $p < 0.001$. **(G)** Overexpression of nesprin-1α-mCherry alone or together with AKAP6β-GFP in undifferentiated (myogenin-negative) C2C12 myoblasts. Co-expression of nesprin-1α and AKAP6β is sufficient for nuclear envelope recruitment of endogenous PCM-1. Scale bars: 20 µm.

562 **Discussion**

563 We conclude that the myogenic transcription factor myogenin controls ncMTOC
564 formation at the nuclear envelope and that myogenin-induced AKAP6β expression is
565 one of the central molecular components required for ncMTOC formation (Figure 8).
566 This conclusion is supported by our findings that 1) myogenin is required to recruit the
567 MTOC proteins PCM-1, pericentrin and AKAP9 to the nuclear envelope in
568 differentiating muscle cells, 2) ectopic myogenin expression is sufficient to promote the
569 formation of an ncMTOC at the nuclear envelope of fibroblasts, and 3) the myogenin-
570 induced isoforms AKAP6β and nesprin-1α are required and sufficient for the
571 recruitment of centrosomal proteins to the nuclear envelope.

572

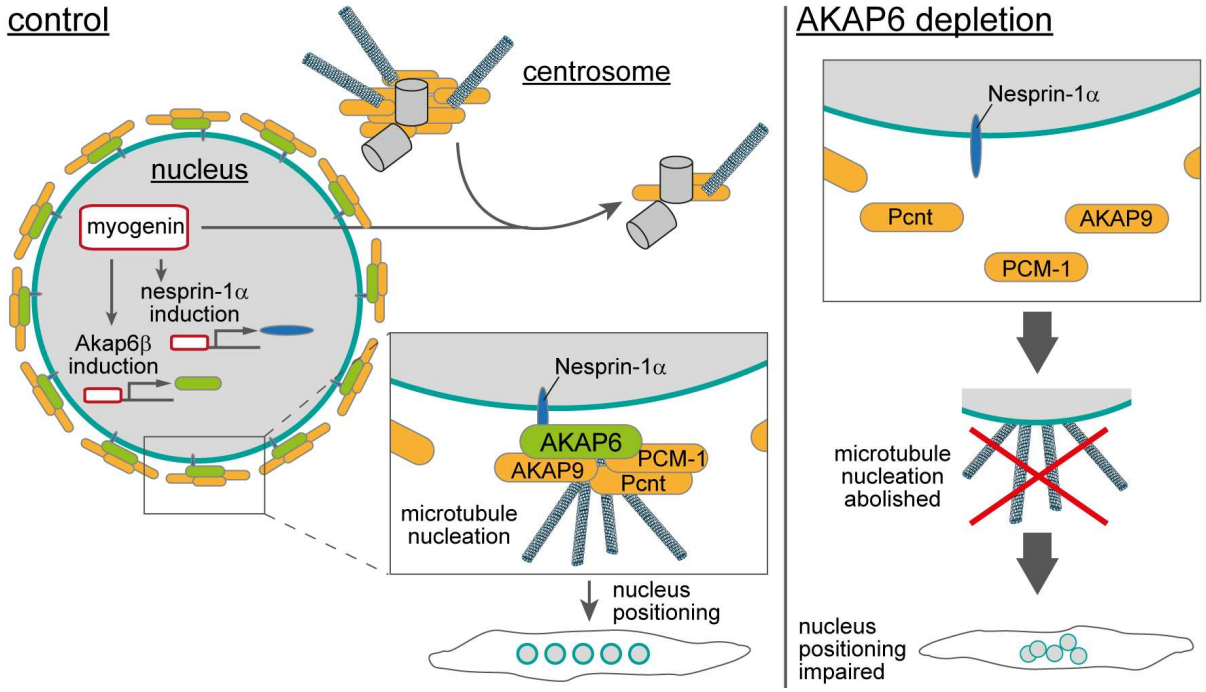

573

574 **Figure 8. Schematic overview of the role of myogenin and AKAP6 in ncMTOC formation.**
575 Myogenin induces expression of AKAP6β which connects centrosomal proteins like pericentrin (Pcnt),
576 AKAP9, and PCM-1 to the nuclear membrane protein nesprin-1α, whose transcription can be induced
577 by myogenin as well. Depletion, overexpression, and co-immunoprecipitation experiments suggest that
578 AKAP6β directly acts as an adapter between centrosomal proteins and nesprin-1α. Yet, other proteins
579 might be involved and the here presented protein complex at the nuclear envelope is hypothetical. At
580 the same time, myogenin is sufficient to attenuate centrosomal MTOC function. AKAP6-dependent
581 anchoring of centrosomal proteins as well as microtubule nucleation from the nuclear envelope are
582 required for correct positioning of nuclei inside differentiating myotubes.

583

584 Formation of ncMTOCs has been associated with cellular differentiation (Sanchez
585 & Feldman, 2017), but a direct regulation of ncMTOC formation by particular
586 differentiation pathways in vertebrate cells has remained elusive. Our results
587 demonstrate that myogenin, which is an essential regulator of terminal differentiation,
588 drives ncMTOC formation in mammalian cells. This shows that terminal differentiation
589 factors can control in vertebrates the switch of dominant MTOC localization from the
590 centrosome to non-centrosomal sites. Notably, MTOC formation at the nuclear
591 envelope occurs also in cells that lack myogenin or cell-type specific transcriptional
592 master regulators of terminal differentiation, such as cardiomyocytes or osteoclasts
593 (Kronebusch & Singer, 1987; Mulari et al., 2003; Zebrowski et al., 2015). A recent study
594 from our lab demonstrated that AKAP6β orchestrates the assembly of the ncMTOC in
595 cardiomyocytes and osteoclasts (Vergarajauregui et al., 2020), validating our findings
596 in skeletal muscle. Therefore, it would be important in future studies to identify
597 transcription factors that bind to AKAP6β and nesprin-1α promoters and regulate the
598 switch from centrosomal to ncMTOC in these cell types. For this purpose, promising
599 cardiomyocyte and osteoclast "transdifferentiation" tools using multiple transcription
600 factors are available (Chang, Cho, Kim, & Kim, 2019; Ieda et al., 2010; Klose, Gossen,
601 & Stamm, 2019; Yamamoto et al., 2015). Additionally, it appears important to
602 determine in future experiments the mechanisms underlying the preferential binding of
603 myogenin to the isoform-specific promoters, considering the abundance of myogenin
604 binding sites (E-boxes) throughout the genome. Notably, isoform upregulation or
605 switching might be a general mechanism that contributes to MTOC regulation during
606 differentiation. This assumption is supported by the recent identification of a spermatid-
607 specific isoform of centrosomin, the *Drosophila* orthologue of CDK5RAP2, which can
608 induce ncMTOC formation at mitochondria (Chen, Buchwalter, Kao, & Megraw, 2017).
609 Moreover, a non-centrosomal isoform of ninein contributes to neuronal differentiation

610 (X. Zhang et al., 2016) and a shorter isoform of pericentrin is upregulated in
611 differentiating cardiomyocytes (Zebrowski et al., 2015).

612 While site-specific anchor proteins for ncMTOCs, such as nesprin-1α, have been
613 identified (Espigat-Georger et al., 2016; Gimpel et al., 2017; Lechler & Fuchs, 2007;
614 Meng, Mushika, Ichii, & Takeichi, 2008), it remained unclear how centrosomal proteins
615 are connected to these site-specific anchors. Previously, it has been reported that
616 overexpression of nesprin-1α in undifferentiated myoblasts is sufficient to recruit an
617 ectopically expressed centrosomal targeting domain of pericentrin and AKAP9 (i.e. the
618 PACT domain) as well as minor amounts of endogenous PCM-1 to the nuclear
619 envelope in a subset of transfected cells (Espigat-Georger et al., 2016; Gimpel et al.,
620 2017). Here, we show that myogenin induced the expression of the large scaffold
621 protein AKAP6, which we prove to be essential for nuclear ncMTOC formation and
622 maintenance, most likely by connecting centrosomal proteins to nesprin-1α. Myogenin
623 preferentially binds and activates the putative promoters of AKAP6β and nesprin-1α
624 isoforms, which are known to be upregulated in differentiated muscle cells (Kapiloff et
625 al., 1999; Michel et al., 2005; Randles et al., 2010). Importantly, ectopic co-expression
626 of AKAP6β and nesprin-1α, but not nesprin-1α alone, was sufficient to recruit
627 endogenous centrosomal proteins in the absence of myogenin.

628 MTOC activity plays a pivotal role for cellular function and altered MTOC function
629 or mutations in genes encoding MTOC proteins are associated with disease such as
630 Emery-Dreifuss muscular dystrophy (*SYNE1*) (Q. Zhang et al., 2007) and
631 Microcephalic osteodysplastic primordial dwarfism, type II (*PCNT*) (Rauch et al., 2008)
632 as well as possibly Long QT syndrome 11 (*AKAP9*) (de Villiers et al., 2014) and Seckel
633 syndrome (*NIN*) (Dauber et al., 2012). In addition, amplified and/or hyperactive
634 centrosomes act as oncogene-like factors (Arnandis et al., 2018; Godinho & Pellman,
635 2014; Godinho et al., 2014; Levine et al., 2017; LoMastro & Holland, 2019). Therefore,

636 it is important to better understand mechanisms that control MTOC activity. Notably,
637 ectopic expression of myogenin in fibroblasts did not only induce ncMTOC formation
638 but also attenuated the centrosomal MTOC. In addition, myogenin expression in
639 fibroblast was only inducing in a subset of cells an ncMTOC. Thus, our cellular systems
640 combined with our bioinformatics approach provides new opportunities to tackle future
641 key questions of MTOC formation such as: What factors increase or decrease
642 efficiency of ncMTOC induction? What post-transcriptional processes contribute to
643 ncMTOC establishment? How are induction of ncMTOC and attenuation of
644 centrosomal MTOC linked?

645 In summary, our findings suggest that key differentiation factors can control the
646 switch from centrosomal MTOC to ncMTOC and cell-type specific adaptor proteins are
647 required to connect centrosomal proteins to anchor proteins at non-centrosomal sites.
648 Conclusively, our study 1) contributes to a better understanding of the striated muscle
649 ncMTOC, 2) presents a mechanistic framework that may be applicable to ncMTOC
650 formation in other cell types and tissues, and 3) provides a cellular system to elucidate
651 further molecular mechanisms inducing the switch from centrosomal to non-
652 centrosomal MTOCs.

653 **Material and Methods**

654 Further information and requests for resources and reagents should be directed to and
655 will be fulfilled by the lead contact, Felix Engel (felix.engel@uk-erlangen.de).

656

657 **Cell lines, differentiation and doxycycline stimulation**

658 The following cell lines have been used in the present study:

Cell Lines	Source	Catalogue number/ Identifier
Mouse: C2C12 myoblast cell line	ATCC	Cat# CRL-1772, RRID: CVCL_0188
Mouse: NIH3T3 fibroblast cell line	ATCC	Cat# CRL-1658, RRID:CVCL_0594
Human: HEK293T cell line	ATCC	Cat# PTA-4488, RRID:CVCL_0045
Human: myoblasts healthy donor	(Holt et al., 2016; Mamchaoui et al., 2011)	N/A
Human: myoblasts carrying SYNE1 mutation	(Holt et al., 2016; Mamchaoui et al., 2011)	N/A

659

660 Reagents used for cell culture are listed in the table below. All cells used in this
661 study were cultured at 37°C in a humidified atmosphere containing 5% CO_2. Growth
662 medium for C2C12, NIH3T3, Hela and Hct116 consisted of high glucose DMEM
663 supplemented with GlutaMAX containing 10% FBS, 1 mM sodium pyruvate, 100 U/ml
664 penicillin and 100 µg/ml streptomycin. C2C12 cells were maintained at 50% confluence
665 to preserve differentiation capacity. For differentiation, cells were cultured to 90%
666 confluence and subsequently changed to differentiation medium (high glucose DMEM
667 with GlutaMAX containing 0.5% FBS and Insulin, Transferrin, Selenium, Sodium
668 Pyruvate Solution (1:1000 of 100x ITS-A).

669 Human myoblasts from a healthy control or from a congenital muscular dystrophy
670 patient carrying a homozygous nonsense mutation within the *SYNE1* gene (nucleotide
671 23560 G>T) were immortalized by Kamel Mamchaoui and Vincent Mouly (Center for
672 Research in Myology, Paris, France) as previously described via transduction with
673 retrovirus vectors expressing hTERT and Cdk4 (Holt et al., 2016; Mamchaoui et al.,
674 2011). Growth medium consisted of DMEM supplemented with GlutaMAX and DMEM
675 199 in a 4:1 ratio containing 20% FBS, 25 µg/ml bovine fetuin, 5 ng/ml recombinant
676 human EGF, 0.5 mg/ml recombinant human FGF-basic, 5 µg/ml recombinant insulin,
677 0.2 µg/ml dexamethasone, and 50 µg/ml gentamicin (Gimpel et al., 2017). To induce
678 differentiation, immortalized myoblasts were grown to ~90% confluence and then
679 changed to Skeletal Muscle Differentiation Medium (PromoCell) containing 50 µg/ml
680 gentamicin. For immunofluorescence analysis of immortalized myoblasts, glass
681 coverslips were coated with Matrigel diluted 1:100 in DMEM.

Cell culture reagent	Source	Catalogue number/ Identifier
0.25% Trypsin/EDTA solution	Sigma Aldrich	Cat# T4049
Dulbecco's Modified Eagle Medium (DMEM), high glucose, GlutaMAX	Thermo Fisher Scientific	Cat# 61965059
DMEM 199 medium	Thermo Fisher Scientific	Cat# 41150
Skeletal Muscle Differentiation Medium	PromoCell	Cat# C-23061
Fetal Bovine Serum (FBS)	biowest	Cat# S1810
Fetal Bovine Serum (FBS), tetracycline free	PAN-Biotech	Cat# P30-3602
Doxycycline hydrochloride	Sigma-Aldrich	Cat# D3447
Horse Serum	Thermo Fisher Scientific	Cat# 16050122
Sodium pyruvate solution	Sigma-Aldrich	Cat# S8636
Penicillin-Streptomycin	Thermo Fisher Scientific	Cat# 15140122
Gentamicin	Thermo Fisher Scientific	Cat# 15750060

Insulin-Transferrin-Selenium-Sodium Pyruvate (ITS-A) (100X)	Thermo Fisher Scientific	Cat# 51300044
Bovine fetuin	Thermo Fisher Scientific	Cat# 10344026
EGF Recombinant Human Protein	Thermo Fisher Scientific	Cat# PHG0311
FGF-Basic (AA 10-155) Recombinant Human Protein	Thermo Fisher Scientific	Cat# PHG0026
Insulin, Human Recombinant	Sigma-Aldrich	Cat# 91077C
Dexamethasone	Sigma-Aldrich	Cat# D4902
Matrigel® hESC-Qualified Matrix, LDEV-free	Corning	Cat# 356277
Fibronectin bovine plasma	Sigma-Aldrich	Cat# F1141

682

683 **Myotube enrichment**

684 C2C12 cells were differentiated in 6-well plates or 10 cm dishes for 4-5 days as
685 described above. To preferentially detach myotubes, cells were washed two times with
686 PBS and treated with pre-warmed 0.0125% Trypsin/EDTA solution (0.25%
687 Trypsin/EDTA stock diluted in PBS) for ~2 min at room temperature. Detachment of
688 myotubes was constantly monitored by phase contrast microscopy. After sufficient
689 myotube detachment was observed, Trypsin/EDTA solution was carefully aspirated
690 and a myotube-enriched suspension was collected by rinsing the plates five times with
691 normal growth medium. Enriched myotubes were then plated on glass coverslips
692 coated with 25 µg/ml fibronectin in PBS for >45 min at 37°C. After 24 h incubation at
693 37°C myotube cultures were subjected to siRNA treatment and/or microtubule
694 regrowth assays.

695

696 **MRF plasmids construction**

697 Primers used to generate fragments are listed in the table below. *Myod* and *Myog*
698 cDNA were obtained by reverse transcription PCR using RNA from C2C12 cells
699 differentiated for 2 days. The cDNAs were then cloned into the peGFP-N1 backbone

700 by Cold Fusion Cloning (System Biosciences, Cat# MC010B-1) following the
701 manufacturer's instruction. Positive clones were identified by restriction digest and
702 Sanger sequencing.

Oligonucleotides	Sequence
Primer: mouse MyoD cold fusion cloning forward	gggatccaccggtcgccaccatggagcttctatcgccgcc
Primer: mouse MyoD cold fusion cloning reverse	tcctcgcccttgctcaccataagcacctgataaatcgcat
Primer: mouse myogenin cold fusion cloning forward	gggatccaccggtcgccaccatggagctgtatgagacatc
Primer: mouse myogenin cold fusion cloning reverse	tcctcgcccttgctcaccatgttgggcatggtttcgtctg

703

704 **Luciferase plasmids construction**

705 Candidate regulatory elements associated with myogenin binding in *Syne1* and *Akap6*
706 genes were identified from ENCODE data accessed through the SCREEN web
707 interface (https://screen.wenglab.org/). Potential promoter regions were amplified from
708 genomic DNA obtained from NIH3T3 cells using the primers listed in the table below.
709 After amplification, promoter fragments were cloned in front of the *Renilla* luciferase
710 ORF (*hRluc*) into the psiCHECK-2 vector (Promega, Cat# C8021; GenBank Accession
711 Number AY535007) using NEBuilder HiFi DNA Assembly Master Mix (New England
712 Biolabs, Cat# E2621L) according to the manufacturer's instructions.

Oligonucleotides	Sequence
Primer: psiCHECK™-2 assembly cloning forward	gctagccaccatggcttc
Primer: psiCHECK™-2 assembly cloning reverse	gtcgagccatgtgagcaaaag
Primer: AKAP6α promoter fragment assembly cloning forward	ttttgctcacatggctcgacgcaaaccatgattattatctaagtc
Primer: AKAP6α promoter fragment assembly cloning forward	tggaagccatggtggctagcaggagatgccttgtttgac
Primer: AKAP6β promoter fragment assembly cloning forward	ttttgctcacatggctcgactacagagaattaatgcttagaaac
Primer: AKAP6β promoter fragment assembly cloning reverse	tggaagccatggtggctagcgcttgcagtgaactgtaatg

Primer: Syne1-giant promoter fragment assembly cloning forward	ttttgctcacatggctcgacactctgtctctttcaacccaaacatc atgaacc
Primer: Syne1-giant promoter fragment assembly cloning reverse	tggaagccatggtggctagcggctgtgccctccctccc
Primer: Syne1-α promoter fragment assembly cloning forward	ttttgctcacatggctcgacgtgtcagattctgactcattg
Primer: Syne1-α promoter fragment assembly cloning reverse	tggaagccatggtggctagctggtcatgcttctaaataaaac

713

714 **Plasmid transfections**

715 Plasmid transfection into NIH3T3 cells was carried out with 500 ng DNA per well of a
716 24-well plate using 1 µl Lipofectamine LTX (Thermo Fisher Scientific, Cat# 15338100)
717 according to the manufacturer's instructions. Transfection complexes were formed by
718 incubating DNA with Lipofectamine LTX in Opti-MEM for 20 min at room temperature.
719 For transfection of luciferase constructs in HEK293T cells, 250 ng luciferase vector
720 and 250 ng myogenin-eGFP or eGFP control plasmid were used per well of a 24-well
721 plate. Transfection complexes were assembled by incubating DNA with PEI MAX
722 (Polysciences, Cat# 24765-1) in a 1:3 ratio in Opti-MEM for 20 min at room
723 temperature.

724

725 **siRNA transfections**

726 Cells were transfected using 2 µl Lipofectamine RNAiMAX reagent (Thermo Fisher
727 Scientific, Cat# 13778150) and 40 nM final siRNA concentration per well of a 24-well
728 plate. Transfection complexes were formed by incubating siRNA with RNAiMAX in
729 Opti-MEM for 20 min at room temperature. C2C12 cells were transfected 24 h prior to
730 induction of differentiation (~50% confluence) and enriched C2C12 myotubes were
731 transfected 24 h after re-plating. NIH3T3 were transfected with siRNA 48 h after
732 plasmid transfection. The following siRNAs have been used in this study:

733

Oligonucleotides and sequences	Source	Catalogue number
siRNA targeting sequence: mouse Myogenin AAUAAAGACUGGUUGCUAUCAAAAA	Integrated DNA technologies	Cat# mm.Ri.Myog.13.1
siRNA targeting sequence: mouse Akap6 GGACUACAUCAAGAACGAATT	Thermo Fischer Scientific	Cat# 4390771 s108732
Negative control (si-ctrl) siRNA	Integrated DNA technologies	Cat# 51-01-14-04

734

735 **Luciferase assay**

736 Luciferase activity was measured in Centro XS^3 LB 960 96-well plate reader
737 luminometer (BertholdTech, #50-6860) using the Dual-Luciferase® Reporter Assay
738 System (Promega, #E1910) according to the manufacturer's instructions. In brief,
739 HEK293T cells were harvested 48h after transfection in passive lysis buffer and stored
740 at -80°C until measurement. Activities of firefly luciferase (*hluc+*, internal control) and
741 *Renilla* luciferase (promoter activation) were measured sequentially for each sample.
742 Values of *Renilla* luciferase activity were normalized to those of firefly luciferase for
743 each measurement.

744

745 **Production of lentiviral vectors**

746 The lentiviral packaging plasmid psPAX2 and the VSV-G envelope plasmid pMD2.G
747 were gifts from Didier Trono (psPAX2: Addgene plasmid #12260;
748 http://n2t.net/addgene:12260; RRID: Addgene_12260; pMD2.G: Addgene plasmid
749 #12259; http://n2t.net/addgene:12259; RRID: Addgene_12259). The transfer plasmids
750 pLenti CMVtight Blast DEST (w762-1) and pLenti CMV rtTA3 Hygro (w785-1) used for
751 creating tetracycline-inducible cell lines were gifts from Eric Campeau (w762-1:
752 Addgene plasmid #26434; http://n2t.net/addgene:26434; RRID: Addgene_26434;
753 w785-1: Addgene plasmid #26730; http://n2t.net/addgene:26730; RRID:
754 Addgene_26730). The coding sequences of human myogenin (gift from Matthew

755 Alexander & Louis Kunkel (Addgene plasmid #78341 ; http://n2t.net/addgene:78341;
756 RRID: Addgene_78341) and mScarlet (Bindels et al., 2017) (gift from Dorus Gadella
757 (Addgene plasmid #85042; http://n2t.net/addgene:85042; RRID: Addgene_85042)
758 were cloned into w762-1 by NEBuilder® HiFi DNA Assembly according to the
759 manufacturer's instructions using the primers indicated in the table below.

760 To produce lentiviral vectors, psPAX2, pMD2.G, and the desired transfer plasmid
761 were transfected in a 1:1:2 ratio into HEK293T cells using PEI MAX. Supernatant
762 containing lentiviral vectors was harvested 72h after transfection, filtered through a
763 0.45 µm filter and aliquots were snap frozen.

764

Oligonucleotides	Sequence
Primer: human myogenin cloning into pLenti CMVtight Blast DEST forward	agccgccaccATGGAGCTGTATGAGACATC
Primer: human myogenin cloning into pLenti CMVtight Blast DEST reverse	ctgccctctccactgcccatGTTGGGCATGGTTTCATC
Primer: mScarlet cloning into pLenti CMVtight Blast DEST forward	tcctggcccaATGGTGAGCAAGGGCGAG
Primer: mScarlet cloning into pLenti CMVtight Blast DEST reverse	ggccgccactgtgctggataTCACTTGTACAGCTCGTCCATGC

765

766 **Generation of stable cell lines**

767 Lentiviral vector aliquots were rapidly thawed at 37°C and diluted in tetracycline-free
768 growth medium containing 10 µg/ml Polybrene (Sigma-Aldrich, Cat# 107689). Cells
769 were transduced overnight in 6-well plates using 1 ml of diluted lentiviral vector. The
770 following morning, medium was refreshed and cells were selected for transgene
771 integration 72h after transduction. We first generated cells expressing a reverse
772 tetracycline activator (rtTA3), which were subsequently transduced with lentiviral
773 vectors carrying the desired transgene to express mScarlet or MYOG-2A-mScarlet

774 under control of a tetracycline responsive element (TRE). After selection, Tet-ON cell
775 lines were used for 20 passages.
776
777 **Immunoprecipitation**
778 Cells were harvested in lysis buffer containing 1% NP-40, 150 mM NaCl, 10% glycerol,
779 5 mM EDTA, 20 mM Tris-HCl (pH 7) and EDTA-free protease inhibitor cocktail
780 (cOmplete™, Roche # 11873580001). After 30 min incubation on ice, samples were
781 sonicated and lysates were cleared by centrifugation at 16000xg for 16 min at 4°C. For
782 immunoprecipitation, 0.5 µg anti-AKAP6 antibody/mg of total protein were added to the
783 lysate and incubated overnight at 4°C on a rotor. Subsequently, antibody complexes
784 were purified by incubation of lysate with Protein A Sepharose® beads (Merck, GE17-
785 5138-01) for 3h rotating at 4°C. Beads were washed three times with cold lysis buffer
786 for 5 min and proteins were eluted from beads by incubation in 2x NuPAGE LDS
787 sample buffer () at 95°C for 5 min. Lysates and immunoprecipitated samples were
788 analyzed by SDS-PAGE (4-12% NuPAGE Novex Bis-Tris gels) under reducing
789 conditions and transferred to a nitrocellulose membrane by wet transfer at 350 mA and
790 <60 V for 1.5 h in 1x transfer buffer (25 mM Tris-HCl, pH 7.5, 192 mM glycine, 0.1%
791 SDS, 10% methanol). The membrane was then blocked with 5% BSA in TBS-T
792 (1×TBS, 0.05% Tween-20) and incubated with the following antibodies:

Antibodies and dilutions	Source	Catalogue number/ Identifier
rabbit polyclonal anti-PCM1 (H-262) dilution: 1:500	Santa Cruz	Cat# sc-67204, RRID:AB_2139591
rabbit polyclonal anti-Akap6 dilution: 1:2000	Sigma-Aldrich	Cat# HPA048741, RRID:AB_2680506
sheep polyclonal anti-rabbit IgG HRP-linked	GE Healthcare	NA934-1ML, RRID:AB_2722659

793 **ChIP-qPCR**

794 Protein and DNA were cross-linked by fixing cells for 10 min at 37°C using 1%
795 formaldehyde in culture medium. Cross-linking was quenched by adding 125 mM
796 glycine and gently agitating the cells for 5 min at room temperature. Then, cells were
797 harvested in ice-cold PBS, centrifuged at 1000xG for 5 min at 4°C, and the resulting
798 pellet was lysed in ChIP lysis buffer (1% SDS, 10 mM EDTA, 50 mM Tris-HCl pH 8.1)
799 for 30 min on ice. After lysis, samples were sonicated for 30 cycles consisting of 20s
800 sonication and 30s pause inside an ice bath. Sonicated samples were centrifuged at
801 4°C for 30 min at 10000xG. A small aliquot of the supernatant was saved as input
802 control and the remaining supernatant was subjected to immunoprecipitation. Samples
803 were diluted 1:5 in RIPA buffer (10x RIPA Millipore, # 20-188; 1:10 dilution in ddH_2O)
804 and incubated overnight at 4°C with 1 µg/ml myogenin antibody (Santa Cruz
805 Biotechnology, #sc-12732 X) or IgG1 isotype control (Thermo Fisher, # 16471482).
806 Protein G agarose beads (Roche #11719416001) pre-blocked with salmon sperm
807 (Thermo Fisher, # 15632011) were used to precipitate antibody complexes from diluted
808 samples. Beads were sequentially washed at 4°C with low salt buffer (0.1% SDS, 1%
809 Triton X-100, 2 mM EDTA, 20 mM Tris-HCl pH 8.0, 150 mM NaCl), high salt buffer
810 (0.1% SDS, 1% Triton X-100, 2 mM EDTA, 20 mM Tris-HCl pH 8.0, 500 mM NaCl),
811 LiCl buffer (0.25 M LiCl, 1% NP-40, 1% Sodium Deoxycholate, 1 mM EDTA, 10 mM
812 Tris-HCl pH 8.0), and TE buffer (10 mM Tris-HCl pH 8.0, 1 mM EDTA). Antibody
813 complexes were eluted by incubating beads for 15 min at 30°C in elution buffer
814 (1% SDS, 100 mM $NaHCO_3$). Eluates were digested with proteinase K and RNAse A
815 and DNA fragments were purified using a PCR purification kit (Macherey-Nagel,
816 #740609).

817 **Immunofluorescence and microscopy**

818 Antibodies used in this study are listed in the table below. Note that the MANNES1E
819 antibody detects different nesprin-1 isoforms (Holt et al., 2016; Randles et al., 2010).
820 However, previous studies have shown that only the nesprin-1α isoform is up-regulated
821 during muscle differentiation (Espigat-Georger et al., 2016; Gimpel et al., 2017; Holt et
822 al., 2016). Prior to fixation, cells were rinsed once with PBS. Cells were fixed either
823 with pre-chilled methanol at -20°C for 3 min or with 4% formaldehyde/PBS for 10 min
824 at room temperature. Formaldehyde-fixed cells were permeabilized with 0.5% TritonX-
825 100/PBS. Prior to antibody staining, samples were blocked for at least 20 min using
826 5% BSA in 0.2% Tween-20 in PBS. Primary antibodies were diluted in blocking reagent
827 and incubated with the sample for 90 min at room temperature or overnight at 4°C.
828 After removal of primary antibody solution and three 5 min washes with 0.1%
829 NP40/PBS, samples were incubated for 60 min with fluorophore-coupled secondary
830 antibodies. DNA was visualized with 0.5 µg/ml DAPI (4′,6′-diamidino-2-phenylindole)
831 in 0.1% NP40/PBS. After DAPI staining cover slips were rinsed once with Millipore-
832 filtered water and then mounted using Fluoromount-G mounting medium. Analysis,
833 image acquisition and high-resolution microscopy were done using a LSM800 confocal
834 laser scanning microscope equipped with an Airyscan detector and the ZEISS Blue
835 software (Carl Zeiss AG, RRID: SCR_013672) with Airyscan image processing.

Antibodies and dilutions	Source	Catalogue number/ Identifier
rabbit polyclonal anti-PCM1 (H-262) dilution: 1:200	Santa Cruz	Cat# sc-67204, RRID:AB_2139591
mouse monoclonal anti-PCM1 (G-6) dilution: 1:200	Santa Cruz	Cat# sc-398365
rabbit polyclonal anti-Akap6 dilution: 1:1000	Sigma-Aldrich	Cat# HPA048741, RRID:AB_2680506
mouse monoclonal anti-nesprin-1 (MANNES1E) dilution: 1:50	G. Morris (Randles et al., 2010)	N/A

mouse monoclonal anti-Myogenin (F5D) dilution 1:500	Santa Cruz	Cat# sc-12732, RRID:AB_627980
mouse monoclonal anti-MyoD1 dilution: 1:500	Millipore	Cat# MAB3878, RRID:AB_2251119
rat anti-α-tubulin dilution: 1:500	Sigma-Aldrich	Cat# T9026, RRID:AB_477593
goat polyclonal anti-Troponin I dilution: 1:500	Abcam	Cat# ab56357, RRID:AB_880622
mouse monoclonal anti-γ-tubulin dilution: 1:100	Santa Cruz	Cat# sc-51715, RRID:AB_630410
rabbit polyclonal anti-Akap9 dilution: 1:200	Sigma-Aldrich	Cat# HPA026109, RRID:AB_1844688
rabbit polyclonal anti-Pericentrin dilution: 1:1000	BioLegend	Cat# PRB-432C, RRID:AB_291635
Donkey anti-Rabbit IgG (H+L) Highly Cross-Adsorbed Secondary Antibody, Alexa Fluor 488 dilution: 1:500	Thermo Fisher Scientific	Cat# A21206
Donkey anti-Rabbit IgG (H+L) Highly Cross-Adsorbed Secondary Antibody, Alexa Fluor 594 dilution: 1:500	Thermo Fisher Scientific	Cat# A21207
Donkey anti-Rabbit IgG (H+L) Highly Cross-Adsorbed Secondary Antibody, Alexa Fluor 647 dilution: 1:500	Thermo Fisher Scientific	Cat# A31573
Donkey anti-Mouse IgG (H+L) Highly Cross-Adsorbed Secondary Antibody, Alexa Fluor 488 dilution: 1:500	Thermo Fisher Scientific	Cat# A21202
Donkey anti-Mouse IgG (H+L) Highly Cross-Adsorbed Secondary Antibody, Alexa Fluor 594 dilution: 1:500	Thermo Fisher Scientific	Cat# A21203
Donkey anti-Mouse IgG (H+L) Highly Cross-Adsorbed Secondary Antibody, Alexa Fluor 647 dilution: 1:500	Thermo Fisher Scientific	Cat# A31571

Donkey anti-Goat IgG (H+L) Highly Cross-Adsorbed Secondary Antibody, Alexa Fluor 647 dilution: 1:500	Thermo Fisher Scientific	Cat# A21447
Donkey anti-Rat IgG (H+L) Highly Cross-Adsorbed Secondary Antibody, Alexa Fluor 594 dilution: 1:500	Thermo Fisher Scientific	Cat# A21209

836

837 **Image analysis**

838 All image analyses were carried out using Fiji (http://fiji.sc, RRID: SCR_002285). For
839 quantification of nuclear envelope coverage, confocal images were transformed into
840 binary images by setting a manual intensity threshold. Regions of interests (ROI) were
841 obtained by detecting nuclei outline via DAPI staining and subsequent transformation
842 of these outlines into 1 µm-wide bands. Coverage was quantified as the percentage of
843 positive pixels inside bands in the binary images. ROIs for measuring intensities at
844 centrosomes were generated by detecting local signal maxima in γ-tubulin channels
845 and subsequent generation of circular ROIs with 1 µm diameter using the maxima as
846 centers.

847 To measure nuclear envelope intensity profiles for nesprin-1α and AKAP6, we first
848 created ROIs by manually detected nuclear outlines using DAPI staining. We then
849 decreased the diameter of these ROIs by 1 µm and used the newly created ROIS as
850 starting points for linear intensity profiles perpendicular to the nuclear outlines.

851

852 **Microtubule regrowth assay**

853 Cells were treated with 5 µM nocodazole (Sigma-Aldrich, Cat# M1404) in culture media
854 for 3 h at 37°C to depolymerize microtubules. To observe microtubule regrowth,
855 nocodazole-containing medium was removed, cells were rinsed three times with cold
856 medium and either fixed (0 min time point) with 4% formaldehyde in PBS for 10 min or
857 immediately transferred to 37°C pre-warmed culture media for the desired length of

858 time followed by formaldehyde fixation. Myotubes were extracted with 1% Triton X-100
859 in PHEM buffer (60 mM PIPES, 25 mM HEPES, 10 mM EGTA, 2 mM MgCl2, pH 6.9)
860 for 30 s at room temperature prior to fixation.
861
862 **Bioinformatics analysis**
863 Data was analyzed with R (http://www.r-project.org/; RRID:SCR_001905) and
864 Bioconductor (http://www.bioconductor.org/, RRID: SCR_006442). Myogenin ChIP-
865 Seq data (GEO accession number: GSE36024) produced within the ENCODE project
866 (Consortium, 2012; Consortium et al., 2020; Yue et al., 2014) were obtained via the
867 UCSC Genome Browser at https://genome.ucsc.edu/index.html (Kent et al., 2002;
868 Rosenbloom et al., 2013). NarrowPeak tracks relative to ChIP-Seq data from four
869 different time points were considered: undifferentiated C2C12 myoblasts as well as
870 C2C12 cultures differentiated for 24 h, 60 h, or 7 days. To identify myogenin promoter
871 binding, peaks were annotated to the Ensembl release 67 mouse genome relying on
872 Bioconductor packages biomaRt v. 2.30.0 (Durinck, Spellman, Birney, & Huber, 2009)
873 and ChIPpeakAnno v. 3.8.9 (Zhu et al., 2010). Genes were considered as myogenin
874 targets if a peak (p-value < 10^{-5}) was localized at a maximum distance of 1 kb from the
875 annotated transcriptional start site.
876 Results of differential expression analysis for RNA-Seq data from C2C12
877 differentiation (GEO accession number: GSE84158) were obtained from the Gene
878 Expression Omnibus (GEO) repository (Doynova et al., 2017). Three sample types
879 were analyzed: C2C12 myoblasts (C1), C2C12 cultures differentiated for 3 days
880 containing myoblasts as well as myotubes (C2), and C2C12 cultures differentiated for
881 7 days and treated with AraC resulting in depletion of proliferating myoblasts (C3).
882 Genes were considered as up-regulated if they exhibited a positive fold change
883 (p-value < 0.05) from C1 to C2 as well as from C1 to C3.

884 Gene expression microarray data for rat heart development were obtained as
885 described previously using the Affymetrix GeneChip RAT 230 Expression Set (Patra
886 et al., 2011). Genes were considered up-regulated if: 1) the corresponding probe set
887 was identified as differentially expressed on the basis of a procedure that accounts for
888 the total area under the profile compared to a constant profile (Di Camillo, Toffolo, Nair,
889 Greenlund, & Cobelli, 2007), and 2) the difference between the maximum expression
890 value over time and the initial one was greater than the difference between the initial
891 value and the minimum value.

892 For Gene Ontology analysis, annotated cellular component terms for each of the
893 potential myogenin targets were retrieved using the search tool at
894 http://geneontology.org/ (Ashburner et al., 2000; The Gene Ontology, 2017). Potential
895 targets annotated with the terms “nuclear membrane” and “nuclear envelope” were
896 considered.

897

898 **QUANTIFICATION AND STATISTICAL ANALYSIS**

899 **Quantification of nesprin-1α positive nuclei**

900 Low levels of nesprin-1 expression can be detected at nuclei of non-differentiated
901 muscle cells using MANNES1E antibody. Prior to scoring of nesprin-1α positive nuclei,
902 we therefore set a threshold for nesprin-1 signal in images of differentiated C2C12 cells
903 by measuring and subtracting maximal nesprin-1 signal intensity in undifferentiated
904 C2C12 cultures.

905

906 **Statistical analysis**

907 As preliminary experiments indicated a large effect size of siRNA treatments and
908 ectopic MRF expression, three biological replicates were performed per experiment
909 (i.e. n = 3). Biological replicate means that cells were freshly plated, treated, fixed and

910 stained, and then analyzed. For each biological replicate, two technical replicates were
911 performed in the sense that two individual wells were processed at the same time.
912 When analyzed, the two technical replicates were scored as one sample.

913 For quantification in C2C12 cells, >500 nuclei were analyzed per condition and
914 biological replicate. For MRF-GFP experiments, >50 GFP-positive cells were analyzed
915 per condition and biological replicate. For nuclear coverage and intensity
916 quantifications of mScarlet and MYOG-mScarlet cells, >100 nuclei or centrosomes
917 were analyzed per condition and pooled from three biological replicates to display
918 distribution in violin plots.

919 Statistical analysis was carried out using GraphPad Prism 5.02 or Prism 8.2.1
920 (La Jolla, USA). Differences between groups were considered statistically significant
921 when the p-value ≤ 0.05. The 95% confidence interval (CI) for the differences between
922 compared groups are reported in the figure legends. Statistical significance of
923 differences between groups was tested using the following:

924

925 **Figures 1F, 1H, S1B, S1C, 5B, 7E:** One-way ANOVA followed by Bonferroni's Post-
926 Hoc test to compare selected pairs of groups.

927 **Figures 2B, 6C, 7B, 7D, 7F:** Student's t-test together with an F-test to assess equality
928 of variances.

929 **Figures 2D, 2F, 2H, 2M, 3B, 3D, 3E, 5D, 5E, 5F:** Kolmogorov-Smirnov test to compare
930 the cumulative distribution of groups.

931

932 **Author Contributions**

933 Conceptualization: R.B., S.V., and F.B.E.

934 Methodology: R.B., S.V., E.L., F.F., and F.B.E.

935 Formal Analysis: E.L., F.F.

936 Investigation: R.B., S.V., F.B., and M.S.

937 Resources: K.M.

938 Writing – Original Draft: R.B. and F.B.E.

939 Writing – Reviewing & Editing: R.B., S.V., F.F., and F.B.E.

940 Visualization: R.B. and F.B.E.

941 Supervision: F.F. and F.B.E.

942 Funding Acquisition: F.F. and F.B.E.

943

944 **Acknowledgments**

945 We acknowledge the Platform for Immortalization of Human Cells at the Institute de
946 Myologie, Paris for the generation and distribution of immortalized human myoblasts.
947 We thank Glenn E. Morris for providing us with nesprin-1 antibody (MANNES1E). We
948 thank the ENCODE consortium, the laboratory of Barbara Wold and the Millard and
949 Muriel Jacobs Genetics and Genomics Laboratory at the California Institute of
950 Technology for providing myogenin ChIP-Seq data. We thank Christina Warnecke for
951 support with ChIP experiments, Marc Stemmler, Eva Bauer, and Thomas Brabletz for
952 their help with luciferase assays and Anna K. Großkopf and Alexander S. Hahn for
953 experimental support. We acknowledge Les Laboratoires Servier for providing
954 illustrations in the Servier Medical Art collection under a Creative Commons Attribution
955 3.0 Unported License (https://creativecommons.org/ licenses/by/3.0/). We thank Anna
956 K. Großkopf, Manfred Frasch, Hanh Nguyen, Thomas U. Mayer, Rosa M. Puertollano,

Payel Das, Marina Leone, Gentian Musa, and Salvador Cazorla-Vazquez for critical reading of the manuscript and all members of the Engel lab for critical discussions.

This work was supported by the Interdisciplinary Centre for Clinical Research Erlangen (IZKF project J42 to F.F.), the Emerging Fields Initiative Cell “Cycle in Disease and Regeneration” (CYDER to F.B.E.) and an ELAN Program Grant (ELAN-16-01-04-1-Vergarajauregui to S.V.) from the Friedrich-Alexander-Universität Erlangen-Nürnberg, by the German Research Foundation (DFG, INST 410/91-1 FUGG and EN 453/12-1 to F.B.E.), and by the Research Foundation Medicine at the University Clinic Erlangen, Germany.

Declaration of Interests

The authors have no conflict of interest to declare.

969 **References**

970 Akhmanova, A., & Steinmetz, M. O. (2015). Control of microtubule organization and dynamics:
971 two ends in the limelight. *Nat Rev Mol Cell Biol, 16*(12), 711-726. doi:10.1038/nrm4084

972 Apel, E. D., Lewis, R. M., Grady, R. M., & Sanes, J. R. (2000). Syne-1, a dystrophin- and
973 Klarsicht-related protein associated with synaptic nuclei at the neuromuscular junction.
974 *J Biol Chem, 275*(41), 31986-31995. doi:10.1074/jbc.M004775200

975 Arnandis, T., Monteiro, P., Adams, S. D., Bridgeman, V. L., Rajeeve, V., Gadaleta, E., . . .
976 Godinho, S. A. (2018). Oxidative Stress in Cells with Extra Centrosomes Drives Non-
977 Cell-Autonomous Invasion. *Dev Cell, 47*(4), 409-424 e409.
978 doi:10.1016/j.devcel.2018.10.026

979 Ashburner, M., Ball, C. A., Blake, J. A., Botstein, D., Butler, H., Cherry, J. M., . . . Sherlock, G.
980 (2000). Gene ontology: tool for the unification of biology. The Gene Ontology
981 Consortium. *Nat Genet, 25*(1), 25-29. doi:10.1038/75556

982 Berkes, C. A., & Tapscott, S. J. (2005). MyoD and the transcriptional control of myogenesis.
983 *Semin Cell Dev Biol, 16*(4-5), 585-595. doi:10.1016/j.semcdb.2005.07.006

984 Bindels, D. S., Haarbosch, L., van Weeren, L., Postma, M., Wiese, K. E., Mastop, M., . . .
985 Gadella, T. W., Jr. (2017). mScarlet: a bright monomeric red fluorescent protein for
986 cellular imaging. *Nat Methods, 14*(1), 53-56. doi:10.1038/nmeth.4074

987 Braun, T., Bober, E., Winter, B., Rosenthal, N., & Arnold, H. H. (1990). Myf-6, a new member
988 of the human gene family of myogenic determination factors: evidence for a gene
989 cluster on chromosome 12. *EMBO J, 9*(3), 821-831. Retrieved from
990 https://www.ncbi.nlm.nih.gov/pubmed/2311584

991 Braun, T., Buschhausen-Denker, G., Bober, E., Tannich, E., & Arnold, H. H. (1989). A novel
992 human muscle factor related to but distinct from MyoD1 induces myogenic conversion
993 in 10T1/2 fibroblasts. *EMBO J, 8*(3), 701-709. Retrieved from
994 https://www.ncbi.nlm.nih.gov/pubmed/2721498

995 Braun, T., & Gautel, M. (2011). Transcriptional mechanisms regulating skeletal muscle
996 differentiation, growth and homeostasis. *Nat Rev Mol Cell Biol, 12*(6), 349-361.
997 doi:10.1038/nrm3118

998 Brodu, V., Baffet, A. D., Le Droguen, P. M., Casanova, J., & Guichet, A. (2010). A
999 developmentally regulated two-step process generates a noncentrosomal microtubule
1000 network in Drosophila tracheal cells. *Dev Cell, 18*(5), 790-801.
1001 doi:10.1016/j.devcel.2010.03.015

1002 Buckingham, M., & Rigby, P. W. (2014). Gene regulatory networks and transcriptional
1003 mechanisms that control myogenesis. *Dev Cell, 28*(3), 225-238.
1004 doi:10.1016/j.devcel.2013.12.020

1005 Chang, Y., Cho, B., Kim, S., & Kim, J. (2019). Direct conversion of fibroblasts to osteoblasts
1006 as a novel strategy for bone regeneration in elderly individuals. *Exp Mol Med, 51*(5), 1-
1007 8. doi:10.1038/s12276-019-0251-1

1008 Chen, J. V., Buchwalter, R. A., Kao, L. R., & Megraw, T. L. (2017). A Splice Variant of
1009 Centrosomin Converts Mitochondria to Microtubule-Organizing Centers. *Curr Biol,*
1010 *27*(13), 1928-1940 e1926. doi:10.1016/j.cub.2017.05.090

1011 Comai, G., & Tajbakhsh, S. (2014). Molecular and cellular regulation of skeletal myogenesis.
1012 *Curr Top Dev Biol, 110*, 1-73. doi:10.1016/B978-0-12-405943-6.00001-4

1013 Conduit, P. T., Wainman, A., & Raff, J. W. (2015). Centrosome function and assembly in animal
1014 cells. *Nat Rev Mol Cell Biol, 16*(10), 611-624. doi:10.1038/nrm4062

1015 Consortium, E. P. (2012). An integrated encyclopedia of DNA elements in the human genome.
1016 *Nature, 489*(7414), 57-74. doi:10.1038/nature11247

1017 Consortium, E. P., Moore, J. E., Purcaro, M. J., Pratt, H. E., Epstein, C. B., Shoresh, N., . . .
1018 Weng, Z. (2020). Expanded encyclopaedias of DNA elements in the human and mouse
1019 genomes. *Nature, 583*(7818), 699-710. doi:10.1038/s41586-020-2493-4

1020 Dammermann, A., & Merdes, A. (2002). Assembly of centrosomal proteins and microtubule
1021 organization depends on PCM-1. *J Cell Biol, 159*(2), 255-266.
1022 doi:10.1083/jcb.200204023

1023 Dauber, A., Lafranchi, S. H., Maliga, Z., Lui, J. C., Moon, J. E., McDeed, C., . . . Hwa, V. (2012).
1024 Novel microcephalic primordial dwarfism disorder associated with variants in the
1025 centrosomal protein ninein. *J Clin Endocrinol Metab, 97*(11), E2140-2151.
1026 doi:10.1210/jc.2012-2150

1027 Davis, R. L., Weintraub, H., & Lassar, A. B. (1987). Expression of a single transfected cDNA
1028 converts fibroblasts to myoblasts. *Cell, 51*(6), 987-1000. doi:10.1016/0092-
1029 8674(87)90585-x

1030 de Villiers, C. P., van der Merwe, L., Crotti, L., Goosen, A., George, A. L., Jr., Schwartz, P. J.,
1031 . . . Corfield, V. A. (2014). AKAP9 is a genetic modifier of congenital long-QT syndrome
1032 type 1. *Circ Cardiovasc Genet, 7*(5), 599-606.
1033 doi:10.1161/CIRCGENETICS.113.000580

1034 Di Camillo, B., Toffolo, G., Nair, S. K., Greenlund, L. J., & Cobelli, C. (2007). Significance
1035 analysis of microarray transcript levels in time series experiments. *BMC Bioinformatics,*
1036 *8 Suppl 1*, S10. doi:10.1186/1471-2105-8-S1-S10

1037 Doynova, M. D., Markworth, J. F., Cameron-Smith, D., Vickers, M. H., & O'Sullivan, J. M.
1038 (2017). Linkages between changes in the 3D organization of the genome and
1039 transcription during myotube differentiation in vitro. *Skelet Muscle, 7*(1), 5.
1040 doi:10.1186/s13395-017-0122-1

1041 Durinck, S., Spellman, P. T., Birney, E., & Huber, W. (2009). Mapping identifiers for the
1042 integration of genomic datasets with the R/Bioconductor package biomaRt. *Nat Protoc,*
1043 *4*(8), 1184-1191. doi:10.1038/nprot.2009.97

1044 Edmondson, D. G., & Olson, E. N. (1989). A gene with homology to the myc similarity region
1045 of MyoD1 is expressed during myogenesis and is sufficient to activate the muscle
1046 differentiation program. *Genes Dev, 3*(5), 628-640. doi:10.1101/gad.3.5.628

1047 Elhanany-Tamir, H., Yu, Y. V., Shnayder, M., Jain, A., Welte, M., & Volk, T. (2012). Organelle
1048 positioning in muscles requires cooperation between two KASH proteins and
1049 microtubules. *J Cell Biol, 198*(5), 833-846. doi:10.1083/jcb.201204102

1050 Espigat-Georger, A., Dyachuk, V., Chemin, C., Emorine, L., & Merdes, A. (2016). Nuclear
1051 alignment in myotubes requires centrosome proteins recruited by nesprin-1. *J Cell Sci,*
1052 *129*(22), 4227-4237. doi:10.1242/jcs.191767

1053 Gimpel, P., Lee, Y. L., Sobota, R. M., Calvi, A., Koullourou, V., Patel, R., . . . Gomes, E. R.
1054 (2017). Nesprin-1alpha-Dependent Microtubule Nucleation from the Nuclear Envelope
1055 via Akap450 Is Necessary for Nuclear Positioning in Muscle Cells. *Curr Biol, 27*(19),
1056 2999-3009 e2999. doi:10.1016/j.cub.2017.08.031

1057 Godinho, S. A., & Pellman, D. (2014). Causes and consequences of centrosome abnormalities
1058 in cancer. *Philos Trans R Soc Lond B Biol Sci, 369*(1650). doi:10.1098/rstb.2013.0467

1059 Godinho, S. A., Picone, R., Burute, M., Dagher, R., Su, Y., Leung, C. T., . . . Pellman, D. (2014).
1060 Oncogene-like induction of cellular invasion from centrosome amplification. *Nature,*
1061 *510*(7503), 167-171. doi:10.1038/nature13277

1062 Hasty, P., Bradley, A., Morris, J. H., Edmondson, D. G., Venuti, J. M., Olson, E. N., & Klein,
1063 W. H. (1993). Muscle deficiency and neonatal death in mice with a targeted mutation
1064 in the myogenin gene. *Nature, 364*(6437), 501-506. doi:10.1038/364501a0

1065 Hinchcliffe, E. H., Miller, F. J., Cham, M., Khodjakov, A., & Sluder, G. (2001). Requirement of
1066 a centrosomal activity for cell cycle progression through G1 into S phase. *Science,*
1067 *291*(5508), 1547-1550. doi:10.1126/science.1056866

1068 Holt, I., Duong, N. T., Zhang, Q., Lam le, T., Sewry, C. A., Mamchaoui, K., . . . Morris, G. E.
1069 (2016). Specific localization of nesprin-1-alpha2, the short isoform of nesprin-1 with a
1070 KASH domain, in developing, fetal and regenerating muscle, using a new monoclonal
1071 antibody. *BMC Cell Biol, 17*(1), 26. doi:10.1186/s12860-016-0105-9

1072 Ieda, M., Fu, J. D., Delgado-Olguin, P., Vedantham, V., Hayashi, Y., Bruneau, B. G., &
1073 Srivastava, D. (2010). Direct reprogramming of fibroblasts into functional
1074 cardiomyocytes by defined factors. *Cell, 142*(3), 375-386.
1075 doi:10.1016/j.cell.2010.07.002

1076 Ishibashi, J., Perry, R. L., Asakura, A., & Rudnicki, M. A. (2005). MyoD induces myogenic
1077 differentiation through cooperation of its NH2- and COOH-terminal regions. *J Cell Biol,*
1078 *171*(3), 471-482. doi:10.1083/jcb.200502101

1079 Kapiloff, M. S., Schillace, R. V., Westphal, A. M., & Scott, J. D. (1999). mAKAP: an A-kinase
1080 anchoring protein targeted to the nuclear membrane of differentiated myocytes. *J Cell*
1081 *Sci, 112 (Pt 16)*, 2725-2736. Retrieved from
1082 http://www.ncbi.nlm.nih.gov/pubmed/10413680

1083 Kent, W. J., Sugnet, C. W., Furey, T. S., Roskin, K. M., Pringle, T. H., Zahler, A. M., & Haussler,
1084 D. (2002). The human genome browser at UCSC. *Genome Res, 12*(6), 996-1006.
1085 doi:10.1101/gr.229102

1086 Khodjakov, A., & Rieder, C. L. (2001). Centrosomes enhance the fidelity of cytokinesis in
1087 vertebrates and are required for cell cycle progression. *J Cell Biol, 153*(1), 237-242.
1088 Retrieved from http://www.ncbi.nlm.nih.gov/pubmed/11285289

1089 Klose, K., Gossen, M., & Stamm, C. (2019). Turning fibroblasts into cardiomyocytes:
1090 technological review of cardiac transdifferentiation strategies. *FASEB J, 33*(1), 49-70.
1091 doi:10.1096/fj.201800712R

1092 Kronebusch, P. J., & Singer, S. J. (1987). The microtubule-organizing complex and the Golgi
1093 apparatus are co-localized around the entire nuclear envelope of interphase cardiac
1094 myocytes. *J Cell Sci, 88 (Pt 1)*, 25-34. Retrieved from
1095 http://www.ncbi.nlm.nih.gov/pubmed/3327863

1096 Leask, A., Obrietan, K., & Stearns, T. (1997). Synaptically coupled central nervous system
1097 neurons lack centrosomal gamma-tubulin. *Neurosci Lett, 229*(1), 17-20.
1098 doi:10.1016/s0304-3940(97)00412-6

1099 Lechler, T., & Fuchs, E. (2007). Desmoplakin: an unexpected regulator of microtubule
1100 organization in the epidermis. *J Cell Biol, 176*(2), 147-154. doi:10.1083/jcb.200609109

1101 Lee, C., Scherr, H. M., & Wallingford, J. B. (2007). Shroom family proteins regulate gamma-
1102 tubulin distribution and microtubule architecture during epithelial cell shape change.
1103 *Development, 134*(7), 1431-1441. doi:10.1242/dev.02828

1104 Lee, S. W., Won, J. Y., Yang, J., Lee, J., Kim, S. Y., Lee, E. J., & Kim, H. S. (2015). AKAP6
1105 inhibition impairs myoblast differentiation and muscle regeneration: Positive loop
1106 between AKAP6 and myogenin. *Sci Rep, 5*, 16523. doi:10.1038/srep16523

1107 Levine, M. S., Bakker, B., Boeckx, B., Moyett, J., Lu, J., Vitre, B., . . . Holland, A. J. (2017).
1108 Centrosome Amplification Is Sufficient to Promote Spontaneous Tumorigenesis in
1109 Mammals. *Dev Cell, 40*(3), 313-322 e315. doi:10.1016/j.devcel.2016.12.022

1110 LoMastro, G. M., & Holland, A. J. (2019). The Emerging Link between Centrosome Aberrations
1111 and Metastasis. *Dev Cell, 49*(3), 325-331. doi:10.1016/j.devcel.2019.04.002

1112 Luders, J. (2020). Nucleating microtubules in neurons: Challenges and solutions. *Dev*
1113 *Neurobiol*. doi:10.1002/dneu.22751

1114 Mamchaoui, K., Trollet, C., Bigot, A., Negroni, E., Chaouch, S., Wolff, A., . . . Mouly, V. (2011).
1115 Immortalized pathological human myoblasts: towards a universal tool for the study of
1116 neuromuscular disorders. *Skelet Muscle, 1*, 34. doi:10.1186/2044-5040-1-34

1117 Meads, T., & Schroer, T. A. (1995). Polarity and nucleation of microtubules in polarized
1118 epithelial cells. *Cell Motil Cytoskeleton, 32*(4), 273-288. doi:10.1002/cm.970320404

1119 Meng, W., Mushika, Y., Ichii, T., & Takeichi, M. (2008). Anchorage of microtubule minus ends
1120 to adherens junctions regulates epithelial cell-cell contacts. *Cell, 135*(5), 948-959.
1121 doi:10.1016/j.cell.2008.09.040

1122 Michel, J. J., Townley, I. K., Dodge-Kafka, K. L., Zhang, F., Kapiloff, M. S., & Scott, J. D. (2005).
1123 Spatial restriction of PDK1 activation cascades by anchoring to mAKAPalpha. *Mol Cell,*
1124 *20*(5), 661-672. doi:10.1016/j.molcel.2005.10.013

1125 Mulari, M. T., Patrikainen, L., Kaisto, T., Metsikko, K., Salo, J. J., & Vaananen, H. K. (2003).
1126 The architecture of microtubular network and Golgi orientation in osteoclasts--major
1127 differences between avian and mammalian species. *Exp Cell Res, 285*(2), 221-235.
1128 doi:10.1016/s0014-4827(03)00033-8

1129 Nabeshima, Y., Hanaoka, K., Hayasaka, M., Esumi, E., Li, S., Nonaka, I., & Nabeshima, Y.
1130 (1993). Myogenin gene disruption results in perinatal lethality because of severe
1131 muscle defect. *Nature, 364*(6437), 532-535. doi:10.1038/364532a0

1132 Nguyen, M. M., McCracken, C. J., Milner, E. S., Goetschius, D. J., Weiner, A. T., Long, M. K.,
1133 . . . Rolls, M. M. (2014). Gamma-tubulin controls neuronal microtubule polarity
1134 independently of Golgi outposts. *Mol Biol Cell, 25*(13), 2039-2050.
1135 doi:10.1091/mbc.E13-09-0515

Nguyen, M. M., Stone, M. C., & Rolls, M. M. (2011). Microtubules are organized independently of the centrosome in Drosophila neurons. *Neural Dev, 6*, 38. doi:10.1186/1749-8104-6-38

Ori-McKenney, K. M., Jan, L. Y., & Jan, Y. N. (2012). Golgi outposts shape dendrite morphology by functioning as sites of acentrosomal microtubule nucleation in neurons. *Neuron, 76*(5), 921-930. doi:10.1016/j.neuron.2012.10.008

Pare, G. C., Easlick, J. L., Mislow, J. M., McNally, E. M., & Kapiloff, M. S. (2005). Nesprin-1alpha contributes to the targeting of mAKAP to the cardiac myocyte nuclear envelope. *Exp Cell Res, 303*(2), 388-399. doi:10.1016/j.yexcr.2004.10.009

Passariello, C. L., Li, J., Dodge-Kafka, K., & Kapiloff, M. S. (2015). mAKAP-a master scaffold for cardiac remodeling. *J Cardiovasc Pharmacol, 65*(3), 218-225. doi:10.1097/FJC.0000000000000206

Patra, C., Diehl, F., Ferrazzi, F., van Amerongen, M. J., Novoyatleva, T., Schaefer, L., . . . Engel, F. B. (2011). Nephronectin regulates atrioventricular canal differentiation via Bmp4-Has2 signaling in zebrafish. *Development, 138*(20), 4499-4509. doi:10.1242/dev.067454

Prosser, S. L., & Pelletier, L. (2015). Centrosome biology: the ins and outs of centrosome assembly. *Curr Biol, 25*(15), R656-659. doi:10.1016/j.cub.2015.06.038

Prosser, S. L., & Pelletier, L. (2020). Centriolar satellite biogenesis and function in vertebrate cells. *J Cell Sci, 133*(1). doi:10.1242/jcs.239566

Randles, K. N., Lam le, T., Sewry, C. A., Puckelwartz, M., Furling, D., Wehnert, M., . . . Morris, G. E. (2010). Nesprins, but not sun proteins, switch isoforms at the nuclear envelope during muscle development. *Dev Dyn, 239*(3), 998-1009. doi:10.1002/dvdy.22229

Rauch, A., Thiel, C. T., Schindler, D., Wick, U., Crow, Y. J., Ekici, A. B., . . . Reis, A. (2008). Mutations in the pericentrin (PCNT) gene cause primordial dwarfism. *Science, 319*(5864), 816-819. doi:10.1126/science.1151174

Rosenbloom, K. R., Sloan, C. A., Malladi, V. S., Dreszer, T. R., Learned, K., Kirkup, V. M., . . . Kent, W. J. (2013). ENCODE data in the UCSC Genome Browser: year 5 update. *Nucleic Acids Res, 41*(Database issue), D56-63. doi:10.1093/nar/gks1172

Ruehr, M. L., Russell, M. A., Ferguson, D. G., Bhat, M., Ma, J., Damron, D. S., . . . Bond, M. (2003). Targeting of protein kinase A by muscle A kinase-anchoring protein (mAKAP) regulates phosphorylation and function of the skeletal muscle ryanodine receptor. *J Biol Chem, 278*(27), 24831-24836. doi:10.1074/jbc.M213279200

Sanchez-Huertas, C., Freixo, F., Viais, R., Lacasa, C., Soriano, E., & Luders, J. (2016). Non-centrosomal nucleation mediated by augmin organizes microtubules in post-mitotic neurons and controls axonal microtubule polarity. *Nat Commun, 7*, 12187. doi:10.1038/ncomms12187

Sanchez, A. D., & Feldman, J. L. (2017). Microtubule-organizing centers: from the centrosome to non-centrosomal sites. *Curr Opin Cell Biol, 44*, 93-101. doi:10.1016/j.ceb.2016.09.003

Sir, J. H., Putz, M., Daly, O., Morrison, C. G., Dunning, M., Kilmartin, J. V., & Gergely, F. (2013). Loss of centrioles causes chromosomal instability in vertebrate somatic cells. *J Cell Biol, 203*(5), 747-756. doi:10.1083/jcb.201309038

1179 Srsen, V., Fant, X., Heald, R., Rabouille, C., & Merdes, A. (2009). Centrosome proteins form
1180 an insoluble perinuclear matrix during muscle cell differentiation. *BMC Cell Biol, 10*, 28.
1181 doi:10.1186/1471-2121-10-28

1182 Tassin, A. M., Maro, B., & Bornens, M. (1985). Fate of microtubule-organizing centers during
1183 myogenesis in vitro. *J Cell Biol, 100*(1), 35-46. Retrieved from
1184 http://www.ncbi.nlm.nih.gov/pubmed/3880758

1185 The Gene Ontology, C. (2017). Expansion of the Gene Ontology knowledgebase and
1186 resources. *Nucleic Acids Res, 45*(D1), D331-D338. doi:10.1093/nar/gkw1108

1187 Toya, M., Kobayashi, S., Kawasaki, M., Shioi, G., Kaneko, M., Ishiuchi, T., . . . Takeichi, M.
1188 (2016). CAMSAP3 orients the apical-to-basal polarity of microtubule arrays in epithelial
1189 cells. *Proc Natl Acad Sci U S A, 113*(2), 332-337. doi:10.1073/pnas.1520638113

1190 Venuti, J. M., Morris, J. H., Vivian, J. L., Olson, E. N., & Klein, W. H. (1995). Myogenin is
1191 required for late but not early aspects of myogenesis during mouse development. *J Cell*
1192 *Biol, 128*(4), 563-576. Retrieved from http://www.ncbi.nlm.nih.gov/pubmed/7532173

1193 Vergarajauregui, S., Becker, R., Steffen, U., Sharkova, M., Esser, T., Petzold, J., . . . Engel, F.
1194 B. (2020). AKAP6 orchestrates the nuclear envelope microtubule-organizing center by
1195 linking golgi and nucleus via AKAP9. *Elife, 9*. doi:10.7554/eLife.61669

1196 Weintraub, H., Tapscott, S. J., Davis, R. L., Thayer, M. J., Adam, M. A., Lassar, A. B., & Miller,
1197 A. D. (1989). Activation of muscle-specific genes in pigment, nerve, fat, liver, and
1198 fibroblast cell lines by forced expression of MyoD. *Proc Natl Acad Sci U S A, 86*(14),
1199 5434-5438. doi:10.1073/pnas.86.14.5434

1200 Yamamoto, K., Kishida, T., Sato, Y., Nishioka, K., Ejima, A., Fujiwara, H., . . . Mazda, O. (2015).
1201 Direct conversion of human fibroblasts into functional osteoblasts by defined factors.
1202 *Proc Natl Acad Sci U S A, 112*(19), 6152-6157. doi:10.1073/pnas.1420713112

1203 Yang, R., & Feldman, J. L. (2015). SPD-2/CEP192 and CDK Are Limiting for Microtubule-
1204 Organizing Center Function at the Centrosome. *Curr Biol, 25*(14), 1924-1931.
1205 doi:10.1016/j.cub.2015.06.001

1206 Yue, F., Cheng, Y., Breschi, A., Vierstra, J., Wu, W., Ryba, T., . . . Mouse, E. C. (2014). A
1207 comparative encyclopedia of DNA elements in the mouse genome. *Nature, 515*(7527),
1208 355-364. doi:10.1038/nature13992

1209 Zebrowski, D. C., Vergarajauregui, S., Wu, C. C., Piatkowski, T., Becker, R., Leone, M., . . .
1210 Engel, F. B. (2015). Developmental alterations in centrosome integrity contribute to the
1211 post-mitotic state of mammalian cardiomyocytes. *Elife, 4*. doi:10.7554/eLife.05563

1212 Zhang, Q., Bethmann, C., Worth, N. F., Davies, J. D., Wasner, C., Feuer, A., . . . Shanahan,
1213 C. M. (2007). Nesprin-1 and -2 are involved in the pathogenesis of Emery Dreifuss
1214 muscular dystrophy and are critical for nuclear envelope integrity. *Hum Mol Genet,*
1215 *16*(23), 2816-2833. doi:10.1093/hmg/ddm238

1216 Zhang, Q., Skepper, J. N., Yang, F., Davies, J. D., Hegyi, L., Roberts, R. G., . . . Shanahan,
1217 C. M. (2001). Nesprins: a novel family of spectrin-repeat-containing proteins that
1218 localize to the nuclear membrane in multiple tissues. *J Cell Sci, 114*(Pt 24), 4485-4498.
1219 Retrieved from http://www.ncbi.nlm.nih.gov/pubmed/11792814

1220 Zhang, X., Chen, M. H., Wu, X., Kodani, A., Fan, J., Doan, R., . . . Walsh, C. A. (2016). Cell-
1221 Type-Specific Alternative Splicing Governs Cell Fate in the Developing Cerebral
1222 Cortex. *Cell, 166*(5), 1147-1162 e1115. doi:10.1016/j.cell.2016.07.025

1223 Zhu, L. J., Gazin, C., Lawson, N. D., Pages, H., Lin, S. M., Lapointe, D. S., & Green, M. R.
1224 (2010). ChIPpeakAnno: a Bioconductor package to annotate ChIP-seq and ChIP-chip
1225 data. *BMC Bioinformatics, 11*, 237. doi:10.1186/1471-2105-11-237

1226

1227

1228 **Figure Supplements**

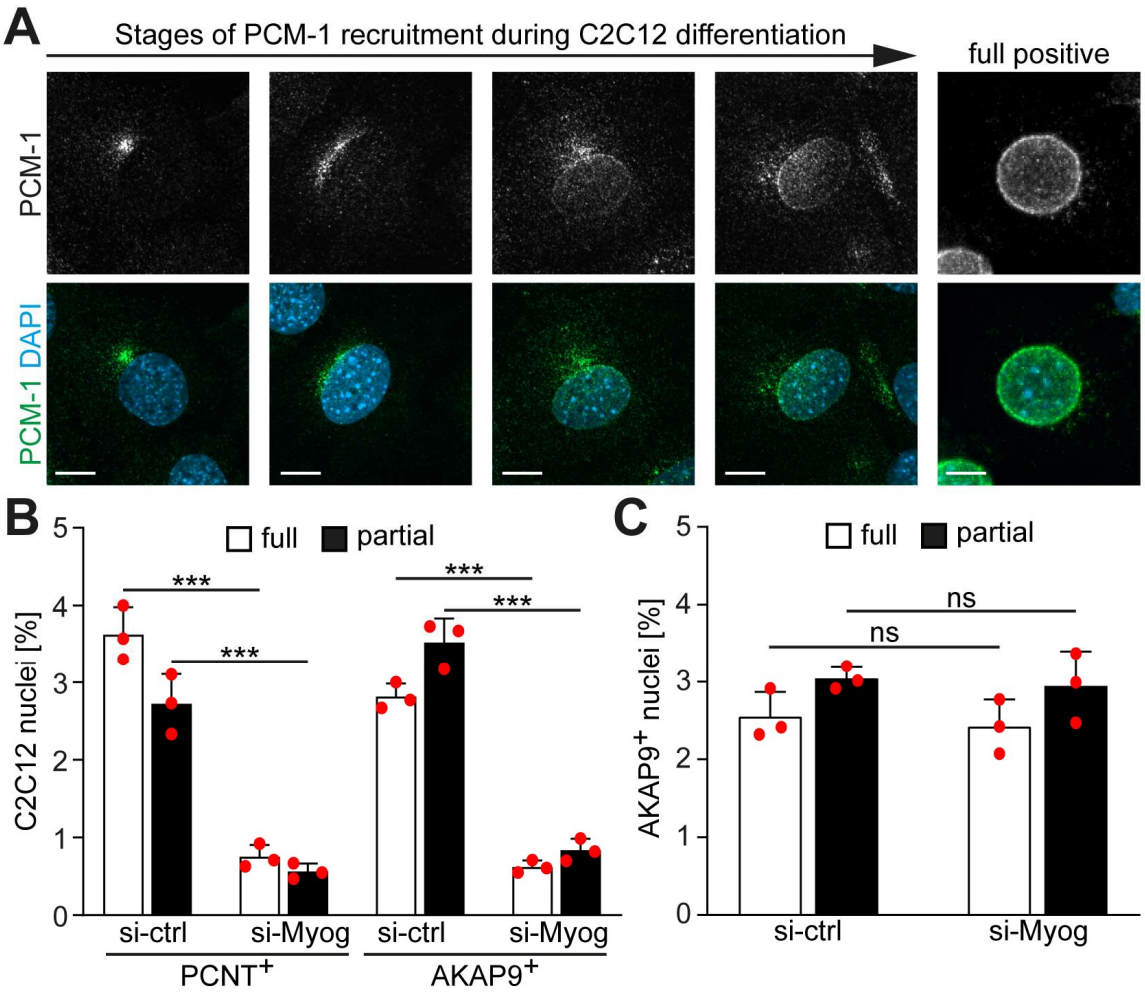

1229

1230 **Figure 1 – figure supplement 1. Centrosomal protein recruitment to the nuclear envelope is**
1231 **gradual.**
1232 **(A)** C2C12 cells were differentiated for 24h and PCM-1 was detected by immunostaining. Different
1233 stages of PCM-1 recruitment are shown with increasing coverage of the nuclear envelope from left to
1234 right. Scale bar = 10 µm. **(B)** A more detailed quantification of pericentrin (PCNT) and AKAP9-positive
1235 nuclei in differentiating C2C12 (treated as described in Figure 1F) showing that myogenin depletion
1236 affects also partial recruitment of PCNT and AKAP9. Data are represented as individual biological
1237 replicates, together with mean ± SD. ***: $p < 0.001$. n = 3. **(C)** C2C12 myoblasts were transfected with
1238 si-ctrl or PCM-1 siRNA (si-PCM1) and differentiated for two days. AKAP9 was detected by
1239 immunostaining and subsequent quantification (H) showed that PCM-1 depletion does not affect AKAP)
1240 positive nuclei. Data are represented as individual biological replicates, together with mean ± SD. ns:
1241 $p > 0.05$. n = 3.

1242

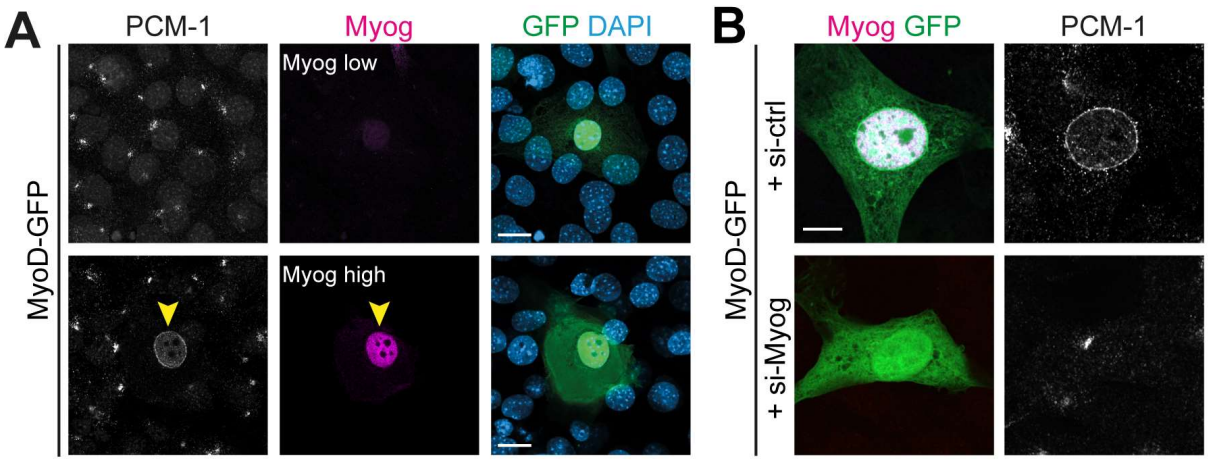

Figure 2 – figure supplement 1. Myogenin is required for MyoD-induced nuclear envelope recruitment of PCM-1.
(A) Three days after ectopic expression of MyoD-GFP in NIH3T3 fibroblasts, immunostaining revealed that nuclear PCM-1 localization is associated with high myogenin (Myog) expression (yellow arrowhead). Scale bars: 10 µm. **(B)** NIH3T3 cells were treated with negative control (si-ctrl) or myogenin (si-Myog) siRNA and 24 h later transfected with a construct encoding MyoD-GFP. Immunofluorescence staining indicates that myogenin is required for MyoD-induced PCM-1 nuclear recruitment. Scale bars: 10 µm.

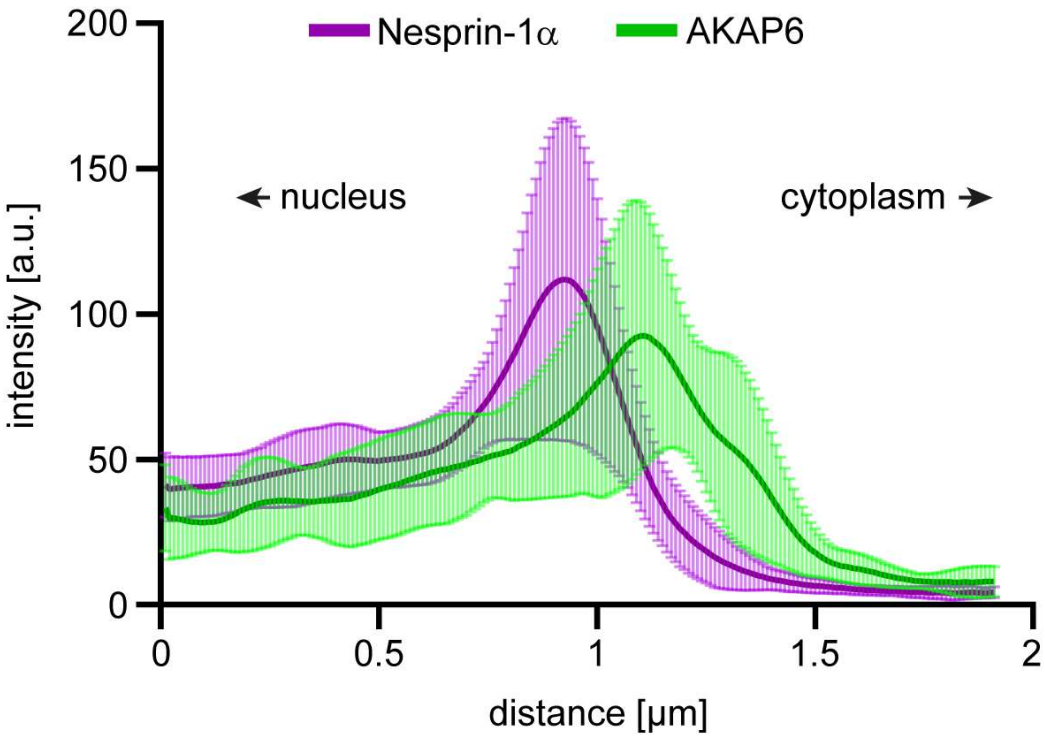

1253

1254 **Figure 4 – figure supplement 1. Quantification of nesprin-1α and AKAP6 signal at the nuclear**
1255 **envelope.**
1256 Differentiated C2C12 cells were immunostained for nesprin-1α and AKAP6. Signal intensity was
1257 quantified as line scan profiles across the nuclear envelope. Ten line scan profiles were obtained in
1258 regular intervals along the nuclear periphery and pooled from ten nuclei. Data are shown as mean ± SD.

1259

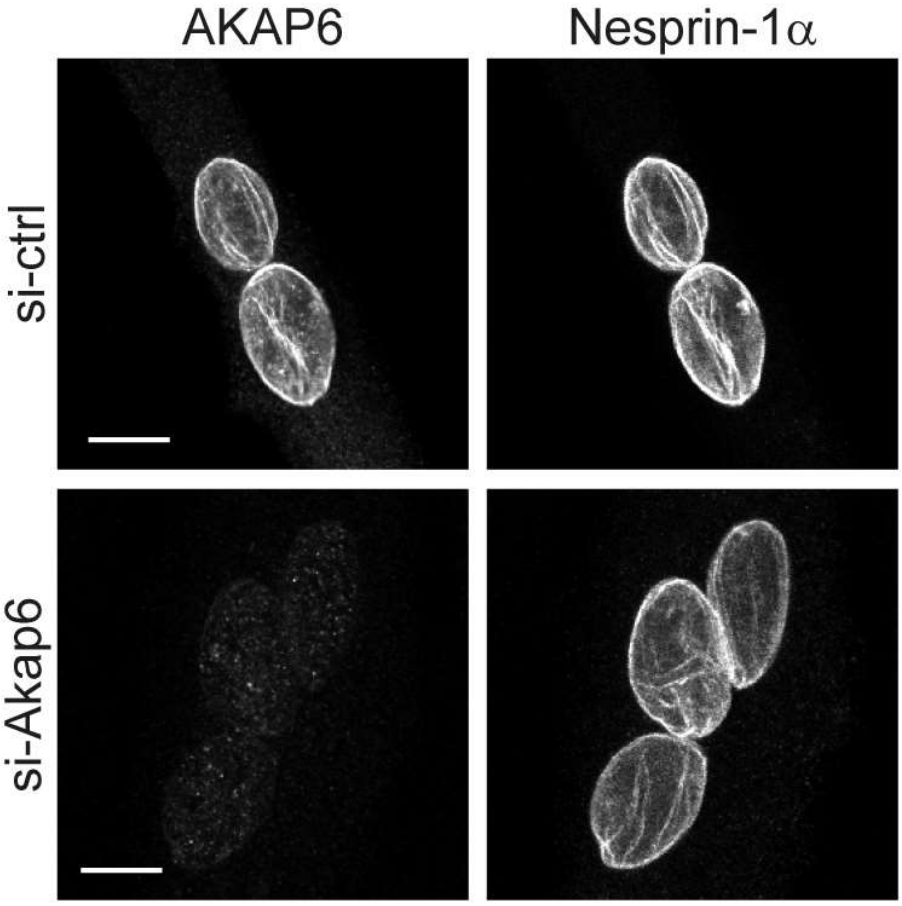

1260

1261 **Figure 5 – figure supplement 1. Akap6 depletion does not affect nesprin-1α.**
1262 Enriched C2C12 myotubes were transfected with scrambled or Akap6-siRNA and immunostained for
1263 Akap6 and nesprin-1α. Scale bars: 10 μm.

1264

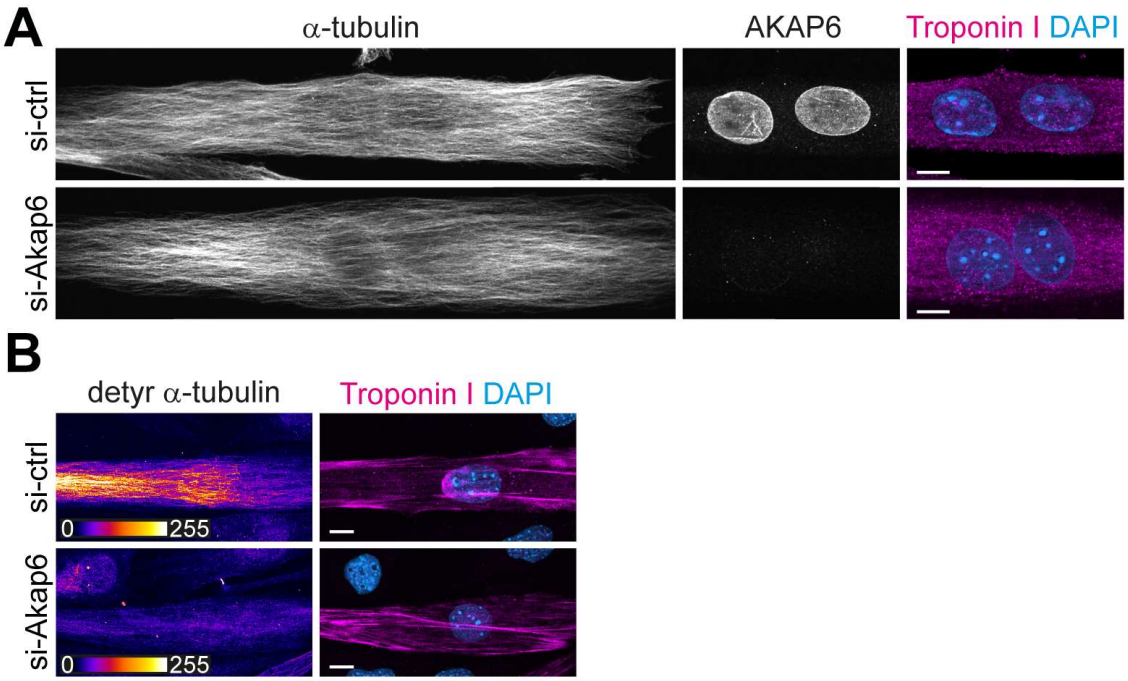

Figure 6 – figure supplement 1. AKAP6 depletion does not affect steady state microtubule organization but reduces detyrosinated microtubules.
(A-B) Enriched C2C12 myotubes (troponin I) were transfected with negative control (si-ctrl) or Akap6 (si-Akap6) siRNA and subsequently analyzed for overall microtubule (α-tubulin) structure (A) or detyrosinated microtubules (detyr α-tubulin). Scale bars: 10 μm.